SIAM J. IMAGING SCIENCES
Vol. 2, No. 2, pp. 670–709


# Scale-Space Analysis of Discrete Filtering over Arbitrary Triangulated Surfaces*

Chunlin Wu†, Jiansong Deng‡, Falai Chen‡, and Xuecheng Tai§

**Abstract.** Discrete filtering of information over triangulated surfaces has proved very useful in computer graphics applications. This technique is based on diffusion equations and has been extensively applied to image processing, harmonic map regularization and texture generating, etc. [C. L. Bajaj and G. Xu, *ACM Trans. Graph.*, 22 (2003), pp. 4–32], [C. Wu, J. Deng, and F. Chen, *IEEE Trans. Vis. Comput. Graph.*, 14 (2008), pp. 666–679]. However, little has been done on analysis (especially quantitative analysis) of the behavior of these filtering procedures. Since in applications mesh surfaces can be of arbitrary topology and the filtering can be nonlinear and even anisotropic, the analysis of the quantitative behavior is a very difficult issue. In this paper, we first present the discrete linear, nonlinear, and anisotropic filtering schemes via discretizing diffusion equations with appropriately defined differential operators on triangulated surfaces, and then use concepts of discrete scale-spaces to describe these filtering procedures and analyze their properties respectively. Scale-space properties such as existence and uniqueness, continuous dependence on initial value, discrete semigroup property, grey level shift invariance and conservation of total grey level, information reduction (also known as topology simplification), and constant limit behavior have been proved. In particular, the information reduction property is analyzed by eigenvalue and eigenvector analysis of matrices. Different from the direct observation of the local filtering to the diffusion equations and other interpretation methods based on wholly global quantities such as energy and entropy, this viewpoint helps us understand the filtering both globally (information reduction as image components shrink) and locally (how the image component contributes to its shrink rate). With careful consideration of the correspondence between eigenvalues and eigenvectors and their features, differences between linear and nonlinear filtering, as well as between isotropic and anisotropic filtering, are discussed. We also get some stability results of the filtering schemes. Several examples are provided to illustrate the properties.

**Key words.** scale-space, discrete filtering, diffusion equation, triangulated mesh surface

**AMS subject classifications.** 65D18, 68U10, 62H35

**DOI.** 10.1137/080722758

## 1. Introduction.

Triangular mesh surfaces have become more and more popular in computer graphics applications for their advantages over parametric and implicit surfaces such as being easy to render, convenient to store, and able to model geometric objects with arbitrary topology. There is a huge volume of literature on modelling and processing of mesh surfaces

*Received by the editors April 29, 2008; accepted for publication (in revised form) February 25, 2009; published electronically May 22, 2009. This work was supported by the National Key Basic Research Project of China (2004CB318000), the Outstanding Youth Grant of NSF of China (60225002), and MOE (Ministry of Education, Singapore) Tier II project T207N2202.

http://www.siam.org/journals/siims/2-2/72275.html

†Division of Mathematical Sciences, School of Physical & Mathematical Sciences, Nanyang Technological University, Singapore (clwu@ntu.edu.sg).

‡Department of Mathematics, University of Science and Technology of China, Hefei, Anhui, People's Republic of China (dengjs@ustc.edu.cn, chenfl@ustc.edu.cn).

§Division of Mathematical Sciences, School of Physical & Mathematical Sciences, Nanyang Technological University, Singapore, and Department of Mathematics, University of Bergen, 5007 Bergen, Norway (tai@math.uib.no).

such as rendering [30], subdivision [6, 66], compression and simplification [15, 54], fairing [10, 12] and editing [1, 63], parametrization and texture mapping [50, 65], and flow simulation on surfaces [49, 53]. In particular, filtering of information defined over surfaces based on diffusion equations has been studied recently and applied to many fields such as image processing, harmonic map regularization and texture generating, and regularization [4, 61]. However, little analysis (especially quantitative analysis) has been done on the behavior of these filtering techniques. Since in applications mesh surfaces can be of arbitrary topology and the filtering can be nonlinear and even anisotropic, the analysis of their quantitative behavior is a hard problem. In this paper, we use discrete scale-space concepts to describe and analyze the linear, nonlinear, and anisotropic filtering procedures, respectively.

Scale-spaces are a basic concept in multiscale representations and analysis of images and have been widely studied in recent decades. The basic idea is to introduce a family of images, namely, the scale-space of the initial image, which progressively become simpler in the sense that significant structures remain while unimportant details vanish. Scale-space representations of images are useful for compression, transmission, segmentation, feature detection, and classification, as well as image matching [21, 28, 29, 36, 38, 44, 45, 52]. The scale-space concept and the multiscale representations of planar images were first introduced for Gaussian convolution by Witkin [60] and were further developed in [3, 13, 14, 18, 23, 24, 26, 27, 28, 32, 33, 34, 35, 36, 42, 48, 51, 64] with deeper discussions and generalizations such as affine scale-space and scale invariant image descriptors; see also a very recent overview [37] and the references therein. Other techniques, such as wavelets, fractals, PDEs, etc., have also been proposed to construct scale-spaces for planar images in recent decades. Among them, PDE-based methods attracted much attention in the past decade for their generality and flexibility [18, 21, 23, 44, 58]. For example, data adaptive multiscale representations of images can be constructed with nonlinear PDEs [44]. Anisotropic scale-spaces [55] can be constructed by introducing a diffusion tensor in PDEs. Besides, PDE-based methods can be relatively easily generalized to nonplanar images, that is, images painted on nonflat manifolds [5, 22]. In the following, we briefly review the scale-space concepts and their properties for PDE-based methods.

The solution of a PDE is defined as the scale-space of the original image (initial data), and the time at which the solution stands is the scale. Different PDEs give different scale-spaces and have different scale-space properties. The linear heat equation determines linear scale-spaces of images. In [23], Koenderink showed that linear scale-spaces satisfy the properties of causality, homogeneity, and isotropy. Causality requires that no additional structure is produced along increasing scale. This is just the information reduction, which can be derived by Fourier analysis. The latter two properties require the spatial invariance of the scale-spaces, which is ensured by the isotropy of the Laplacian operator. Other properties of linear scale-spaces include linearity, grey shift invariance, and the semigroup property [33, 34, 35], scale theorems for zero crossings [64], critical point theory [14, 26, 27, 28, 32], and the entropy property of scale-spaces [51], as well as the global and local topological structure property [48]. However, in linear scale-spaces, edges of images are blurred due to the homogeneity and isotropy criteria, which bring difficulties for posterior edge detection and other applications. By noticing such limitations, Perona and Malik proposed a nonlinear diffusion PDE model to study the multiscale representations (scale-spaces) of images [44]. In that model, an image

edge strength related diffusion coefficient (diffusivity) $c(|\nabla u|)$ is introduced. Different diffusion rates are assigned to different locations. Since the diffusion coefficient $c$ is designed to be a decreasing function of the gradient of the image intensity, blurring is much less at image edges than at other locations. This results in a relative edge enhancement effect. Furthermore, the homogeneity and isotropy criteria are no longer satisfied and are replaced by two new ones, i.e., immediate localization and piecewise smoothing. This is a general framework where the diffusivity $c(|\nabla u|) = c(s)$ can be chosen according to concrete applications. In their paper, Perona and Malik gave two classical diffusivities. The Perona–Malik models were later analyzed and improved by some other researchers [7, 62]. Although the models were discovered to be ill-posed, they have great success in numerical experiments. This is the so-called Perona–Malik paradox. Many authors have tried to explain this paradox; see [20] and the references in [2]. At present, "This phenomenon is still unexplained." [2] In spite of this, it seems that smoothing/enhancement diffusivities behave quite safely and successfully in real calculations. Hence researchers have designed many diffusivities for different applications; see [2, 19] and the references therein. Another well-known nonlinear processor is total variation (TV) minimization [47]. Different from the Perona–Malik framework, TV minimization, or TV regularization, was proposed originally as a variational model, although it is usually finally transformed into a PDE (Euler–Lagrange equation) to solve. TV has shown its power in image processing and was studied extensively; see [8, 9, 43] and the references therein. By introducing a diffusion tensor, Weickert discussed scale-spaces determined by an anisotropic diffusion equation and their properties [55]. Since in applications signals are mostly discrete and scale-space evolutions are computed at exclusively finite number of scales, discrete scale-spaces were proposed in [31, 33] and have become more and more favorable. Various discrete versions of linear scale-spaces were studied in [11]. Weickert and Benhamouda derived semidiscrete and discrete nonlinear scale-spaces and the corresponding properties [56, 57]. A systematic study and analysis of continuous, semidiscrete, and discrete scale-spaces of planar images can be found in [58]. Under some assumptions, the author established a series of scale-space properties such as existence and uniqueness, continuous dependence on initial data, average grey level invariance, information reduction, and constant limit behavior. It should be noticed that these ordinary assumptions for planar images defined on regular grids do not hold for data on general triangulated surfaces.

In this paper, we focus on the analysis of discrete linear, nonlinear, and anisotropic filtering techniques over triangulated surfaces using discrete scale-space concepts. We first give some notation in section 2. In section 3 we present the diffusion models over smooth manifolds. After defining differential operators on triangulated surfaces, we derive our discrete filtering schemes in section 4. The derivation is actually equivalent to the finite volume method (FVM) used in [61]. These discrete filtering schemes are then expressed in section 5 as discrete scale-spaces, from which we study the scale-space properties such as existence and uniqueness, continuous dependence on initial value, the grey level shift invariance property, the discrete semigroup property, information reduction, and limit behavior. As one will see, the proofs of these properties are much more difficult than those of scale-spaces for planar images due to the irregularity of triangular meshes. Examples and discussions are provided in section 6 to support our analysis. We finally conclude the paper with some future work.

**2. Notation.** Assume that $M$ is a triangulated surface with arbitrary topology in $\mathbb{R}^3$. The set of vertices, the set of edges, and the set of face triangles of $M$ are denoted as $\{v_i : i = 0, 1, \ldots, \mathrm{V}-1\}$, $\{e_i : i = 0, 1, \ldots, \mathrm{E}-1\}$, and $\{\tau_i : i = 0, 1, \ldots, \mathrm{T}-1\}$, respectively. Here V, E, and T are the numbers of vertices, edges, and triangles of the triangulated surface, respectively. We explicitly denote an edge $e$ whose endpoints are $p, q$ as $[p, q]$. Similarly, a triangle $\tau$ whose vertices are $p, q, r$ is denoted as $[p, q, r]$. If $v$ is an endpoint of an edge $e$, then we denote it as $v \prec e$. Similarly, that $e$ is an edge of a triangle $\tau$ is denoted as $e \prec \tau$; that $v$ is a vertex of a triangle $\tau$ is denoted as $v \prec \tau$ (see [16]). For a given triangle $\tau$, its barycenter is denoted by $BC(\tau)$. The barycenter of an edge $e$ is denoted by $BC(e)$, while the barycenter of a vertex $v$ is itself ($BC(v) = v$). Let $N_1(i)$ be the 1-neighborhood of vertex $v_i$. It is the set of indices of vertices that are connected to $v_i$. Let $D_1(i)$ be the 1-disk of the vertex $v_i$. $D_1(i)$ is the set of triangles with $v_i$ being one of their vertices. It should be pointed out that the 1-disk of a boundary vertex is topologically just a half-disk.

For each vertex $v_i$, we define a piecewise linear function $\phi_i$ such that $\phi_i(v_j) = \delta_{ij}$, $i, j = 0, 1, \ldots, \mathrm{V}-1$, where $\delta_{ij}$ is the Kronecker delta. $\{\phi_i : i = 0, 1, \ldots, \mathrm{V}-1\}$ has the following properties:

1. local support: $\mathrm{supp}\phi_i = D_1(i)$;
2. nonnegativity: $\phi_i \geq 0$, $i = 0, 1, \ldots, \mathrm{V}-1$;
3. partition of unity: $\sum_{0 \leq i \leq \mathrm{V}-1} \phi_i \equiv 1$.

We can use $\{\phi_i : i = 0, 1, \ldots, \mathrm{V}-1\}$ to build piecewise linear functions on $M$ when function values are known only at the vertices of $M$ (this is the most common case). Suppose $u$ reaches value $u_i$ at vertex $v_i$, $i = 0, 1, \ldots, \mathrm{V}-1$. Then $u(p) = \sum_{0 \leq i \leq \mathrm{V}-1} u_i \phi_i(p)$ for any $p \in M$. Similarly, piecewise linear vector-valued functions $(u_1(p), u_2(p), \ldots, u_d(p))$ on $M$ can be defined. In some applications, we also have piecewise constant function (vector) over $M$; that is, a single value (vector) is assigned to each triangle of $M$ [16].

We now introduce two concepts called dual mesh and control cell, which help to build divergence operators on triangle meshes. For the mesh $M$, a *barycentric dual* is formed by connecting the barycenter and the middle point of each edge in each triangle, as illustrated in Figure 1(a). The original mesh $M$ consists of black lines, while the dual mesh is in blue. Based on the concept of dual meshes, one can assign a *control cell* $C_i$ to each vertex $v_i$ of $M$ [41]. The control cell of a vertex $v_i$ is part of its 1-disk which is near to $v_i$ in the dual mesh. Figure 1(b) shows the control cell $C_i$ for an interior vertex $v_i$ of the original mesh, while Figure 1(c) shows the control cell for a boundary vertex. For the interior vertex $v_i$, the boundary of $C_i$ is

$$\partial C_i = \bigcup_{\tau \in D_1(i)} \bigcup_{v_i \prec e \prec \tau} [BC(e), BC(\tau)]. \tag{2.1}$$

For the boundary vertex, the boundary of the control cell is

$$\partial C_j = \left( \bigcup_{\tau \in D_1(j)} \bigcup_{v_j \prec e \prec \tau} [BC(e), BC(\tau)] \right) \bigcup \left( \bigcup_{v_j \prec e \subseteq \partial M} [BC(v_j), BC(e)] \right), \tag{2.2}$$

where $\partial M$ is the boundary of $M$. We point out that orientations of intervals such as $[BC(e), BC(\tau)]$ should be considered in a consistent way as the clockwise or counterclockwise orientation of the control cell.

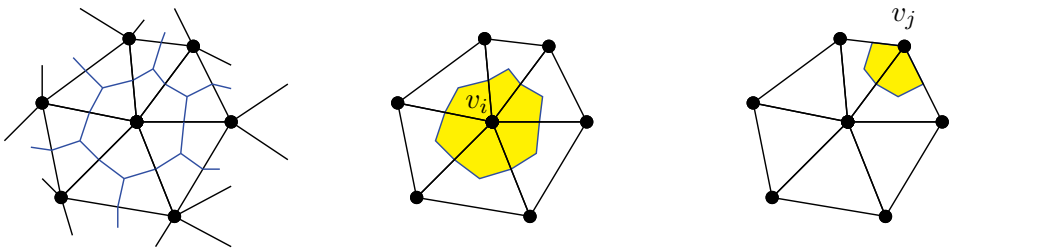


(a) a mesh and its barycentric dual mesh

(b) control cell of an interior vertex

(c) control cell of a boundary vertex

**Figure 1.** *Dual mesh and control cells.*

**3. Diffusion equations on smooth 2-manifolds.** In this section we first introduce some basic concepts for general smooth 2-manifolds, such as tangent space, integration, and differential operators [4, 40, 59]. We then present several diffusion equations on smooth manifolds, which will be discretized in the next section to construct our discrete filtering schemes on triangulated surfaces.

**3.1. Integration, gradient, and divergence on smooth 2-manifolds.** Assume that $\mathcal{M} \subset \mathbb{R}^3$ is a 2-dimensional smooth manifold and that $\{U_\alpha, x_\alpha\}_{\alpha\in\mathcal{A}}$ for some index set $\mathcal{A}$ is the differential structure. $\{U_\alpha, x_\alpha\}_{\alpha\in\mathcal{A}}$ can be viewed as a piecewise parametrization of $\mathcal{M}$. We explicitly denote the local coordinate $U_\alpha$ as $(\xi^1, \xi^2)$. For a given point $x \in x_\alpha(U_\alpha) \subset \mathcal{M}$, the tangent space $T_x\mathcal{M}$ is spanned by $\{\frac{\partial}{\partial\xi^1}, \frac{\partial}{\partial\xi^2}\}$. It should be pointed out that the space $T_x\mathcal{M}$ does not depend on parametrization, although its basis $\{\frac{\partial}{\partial\xi^1}, \frac{\partial}{\partial\xi^2}\}$ does. Different parametrizations (or different differential structures) give different bases of $T_x\mathcal{M}$. We use $T\mathcal{M} = \{X = X(x) : x \in \mathcal{M},\, X(x) \in T_x\mathcal{M}\}$ to denote the set of tangent vector fields.

As $\mathcal{M}$ is embedded in Euclidean space, the differential structure $\{U_\alpha, x_\alpha\}_{\alpha\in\mathcal{A}}$ gives a natural (induced) Riemannian metric tensor $\mathbf{g}$ on $\mathcal{M}$ as follows:

$$\mathbf{g} = (\mathbf{g}_{ij}) = \left( \left\langle \frac{\partial}{\partial\xi^i}, \frac{\partial}{\partial\xi^j} \right\rangle_x \right), \tag{3.1}$$

where $\langle , \rangle$ (in this paper we sometimes also use $\cdot$) is the inner product in Euclidean space, $\mathbb{R}^3$. The tensor $\mathbf{g}$, which is a symmetric and positive definite matrix depending on $x \in \mathcal{M}$, determines a bilinear form on the tangent space $T_x\mathcal{M}$. One can calculate the inner product of any two vectors on $T_x\mathcal{M}$ using the bilinear form.

With the Riemannian metric $\mathbf{g}$, we can define integration on $\mathcal{M}$. Let $f$ be a function on $\mathcal{M}$, and let $\{\varphi_\alpha\}_{\alpha\in\mathcal{A}}$ be a partition of unity on $\mathcal{M}$ with support $\varphi_\alpha \subset U_\alpha$. Then the integration on $\mathcal{M}$ is defined as

$$\int_{\mathcal{M}} f d\mathcal{M} = \sum_\alpha \int_{U_\alpha} \varphi_\alpha f(x_\alpha) \sqrt{\det \mathbf{g}}\, d\xi^1 d\xi^2, \tag{3.2}$$

where $\sqrt{\det \mathbf{g}}\, d\xi^1 d\xi^2$ is the volume form of $\mathcal{M}$. Based on (3.2), we can further define inner

products of two functions $f_1, f_2$ on $\mathcal{M}$ and two vector fields $X_1, X_2$ on $T\mathcal{M}$:

$$(f_1, f_2)_{\mathcal{M}} = \int_{\mathcal{M}} f_1 f_2 d\mathcal{M},$$
$$(X_1, X_2)_{T\mathcal{M}} = \int_{\mathcal{M}} \langle X_1, X_2 \rangle d\mathcal{M}.$$

Moreover, we can express the integration along a curve (a 1-dimensional submanifold) $\mathcal{N} \subset \mathcal{M}$ using local coordinates. Let $\{V_\alpha, \xi_\alpha\}_{\alpha \in \mathcal{A}}$ be the piecewise parametrization of the local coordinates of $\mathcal{N}$ in $U_\alpha$, where $V_\alpha$ is an open set in $\mathbb{R}$. $V_\alpha$ is possibly empty for some $\alpha$. We denote the local coordinate of $V_\alpha$ as $\eta$, that is, $\xi_\alpha = (\xi_\alpha^1(\eta), \xi_\alpha^2(\eta))$. Then the integration of $f$ along $\mathcal{N}$ is

$$\int_{\mathcal{N}} f d\mathcal{N} = \sum_\alpha \int_{V_\alpha} \varphi_\alpha f(x_\alpha(\xi_\alpha)) \sqrt{\mathbf{g}_{ij} \frac{\partial \xi_\alpha^i}{\partial \eta} \frac{\partial \xi_\alpha^j}{\partial \eta}} d\eta = \sum_\alpha \int_{V_\alpha} \varphi_\alpha f(x_\alpha) \left| \frac{\partial x_\alpha}{\partial \eta} \right| d\eta, \tag{3.3}$$

where $|\frac{\partial x_\alpha}{\partial \eta}| = \sqrt{\langle \frac{\partial x_\alpha}{\partial \eta}, \frac{\partial x_\alpha}{\partial \eta} \rangle} = \sqrt{\frac{\partial x_\alpha}{\partial \eta} \cdot \frac{\partial x_\alpha}{\partial \eta}}$. Here (and below) we use the Einstein summation notation.

In the following we introduce the gradient and divergence operators $\nabla_{\mathcal{M}}$ and $\mathrm{div}_{\mathcal{M}}$ on $\mathcal{M}$, which will be used to construct our diffusion equations. Suppose $f \in C^1(\mathcal{M})$ (meaning $f(x) = f(x_\alpha(\xi^1, \xi^2))$ is $C^1$ differentiable with respect to $\xi^1, \xi^2$). Let $(\mathbf{g}^{ij})$ be the inverse of the metric tensor $(\mathbf{g}_{ij})$. The gradient of $f$ is then defined to be

$$\nabla_{\mathcal{M}} f = \mathbf{g}^{ij} \frac{\partial f}{\partial \xi^j} \frac{\partial}{\partial \xi^i}; \tag{3.4}$$

that is,

$$(\nabla_{\mathcal{M}} f)^i = \partial^i f = \mathbf{g}^{ij} \frac{\partial f}{\partial \xi^j}.$$

The component $(\nabla_{\mathcal{M}} f)^i$ along $\frac{\partial}{\partial \xi^i}$ is the change rate of $f$ with respect to $\xi^i$ [4].

We similarly have the divergence of a vector field $X = X^i \frac{\partial}{\partial \xi^i}$ in local coordinates as

$$\mathrm{div}_{\mathcal{M}} X = \frac{1}{\sqrt{\det \mathbf{g}}} \frac{\partial}{\partial \xi^i} (\sqrt{\det \mathbf{g}} X^i). \tag{3.5}$$

Note that $\nabla_{\mathcal{M}} f$ and $\mathrm{div}_{\mathcal{M}} X$ do not depend on the local coordinates, although we use the coordinates to express them. On manifolds, we also have the divergence theorem. Suppose $\mathcal{M}$ has a boundary $\partial\mathcal{M}$; then

$$\int_{\mathcal{M}} \mathrm{div}_{\mathcal{M}} X d\mathcal{M} = \int_{\partial\mathcal{M}} \langle X, \vec{n} \rangle d\partial\mathcal{M} \tag{3.6}$$

for any vector field $X$, where $\vec{n}$ is the intrinsic outward normal vector of $\partial\mathcal{M}$ on the tangent space.

**3.2. Diffusion equations on smooth manifolds.** We now present several diffusion equations on $\mathcal{M}$ via the above defined differential operators. We assume that the initial function defined on $\mathcal{M}$ is $f(x)$. Also we set Neumann boundary conditions in the following equations. If $\mathcal{M}$ has no boundary, these boundary conditions are ignored automatically.

**3.2.1. Linear diffusion.** The linear diffusion equation is as follows:

$$\begin{cases} \frac{\partial u}{\partial t} = \operatorname{div}_{\mathcal{M}} \nabla_{\mathcal{M}} u, \\ \frac{\partial u}{\partial \vec{n}}|_{\partial \mathcal{M}} = 0, \\ u(x,0) = f(x). \end{cases} \tag{3.7}$$

If $\mathcal{M}$ degenerates to a planar domain, the corresponding linear equation is just the classical heat equation which is widely applied in planar image processing, especially linear scale-space construction of planar images [11, 18, 23].

**3.2.2. Nonlinear diffusion.** A general nonlinear diffusion model is

$$\begin{cases} \frac{\partial u}{\partial t} = \operatorname{div}_{\mathcal{M}}(g(|\nabla_{\mathcal{M}} u|)\nabla_{\mathcal{M}} u), \\ \frac{\partial u}{\partial \vec{n}}|_{\partial \mathcal{M}} = 0, \\ u(x,0) = f(x), \end{cases} \tag{3.8}$$

where $g(\cdot)$ is a bounded nonnegative continuous and monotonically descending function. There are many choices for the diffusivity $g = g(s)$ which have been widely used in planar image processing; see [2, 8, 9, 19, 43, 44, 47] and the references therein. In Table 1 we list several frequently used diffusivities, together with $g(s) + sg'(s)$ for each $g(s)$. All of them benefit from the good edge-preserving (or even edge-enhancement) property and have had great success in image restoration.

**Table 1**

*Several choices for $g$ and corresponding $g + sg'$, where $\beta$ is a small positive number.*

| Name | (Regularized) TV [47] | Perona–Malik 1 [44] | Perona–Malik 2 [44] | (Regularized) BFB [19] |
|---|---|---|---|---|
| $g(s)$ | $\frac{1}{\sqrt{s^2+\beta}}$ | $\frac{1}{1+(\frac{s}{K})^2}$ | $\exp(-\frac{1}{2}(\frac{s}{K})^2)$ | $\frac{1}{s^2+\beta}$ |
| $g(s)+sg'(s)$ | $\frac{\beta}{(\sqrt{s^2+\beta})^3}$ | $\frac{1-(\frac{s}{K})^2}{(1+(\frac{s}{K})^2)^2}$ | $\frac{1-(\frac{s}{K})^2}{\exp(\frac{1}{2}(\frac{s}{K})^2)}$ | $\frac{\beta-s^2}{(s^2+\beta)^2}$ |

We now offer some comments on the choice of diffusivities. As revealed in many works on planar image processing (e.g., [2, 19]), $g(s)$ describes the diffusion coefficient along the tangential directions of the level sets of the image, while $g(s) + sg'(s)$ gives the diffusion along the normal directions. Therefore, one can design the form of $g(s)$ according to the concrete problem in hand. The considerations on $g(s)$ may include $\lim_{s\to 0} g(s)$, $\lim_{s\to 0} g(s) + sg'(s)$, $\lim_{s\to\infty} g(s)$, $\lim_{s\to\infty} g(s) + sg'(s)$, and even $\lim_{s\to 0} \frac{g(s)}{g(s)+sg'(s)}$ and $\lim_{s\to\infty} \frac{g(s)}{g(s)+sg'(s)}$, indicating the behavior of the diffusion for different image features; see [2] for details. Since negative diffusion is not stable, the PDE (3.8) associated with the latter three diffusivities in the table is actually ill-posed. However, numerical schemes are demonstrated to be stable, as mentioned in the introduction.

**3.2.3. Anisotropic diffusion.** The anisotropic diffusion model generalizes the linear and nonlinear diffusion models. Assume that $\{e_1(x), e_2(x)\} \subset T\mathcal{M}$ are two orthonormal vector fields in the tangent space. The anisotropic diffusion equation reads as

$$\begin{cases} \frac{\partial u}{\partial t} = \mathrm{div}_{\mathcal{M}}(g_1(|\nabla_{\mathcal{M}} u|)(\nabla_{\mathcal{M}} u \cdot e_1)e_1 + g_2(|\nabla_{\mathcal{M}} u|)(\nabla_{\mathcal{M}} u \cdot e_2)e_2), \\ (g_1(|\nabla_{\mathcal{M}} u|)(\nabla_{\mathcal{M}} u \cdot e_1)e_1 + g_2(|\nabla_{\mathcal{M}} u|)(\nabla_{\mathcal{M}} u \cdot e_2)e_2) \cdot \vec{n}|_{\partial\mathcal{M}} = 0, \\ u(x,0) = f(x), \end{cases} \tag{3.9}$$

where the functions $g_1, g_2$ are bounded, nonnegative, and monotonically descending continuous, indicating diffusion rates along $e_1, e_2$. One can similarly borrow the diffusivities from the planar image processing for $g_1$ and $g_2$. Since in many applications (such as texture generating [61] and the image anti-aliasing on triangulated surfaces; see the examples in section 6) the geometry of the surface plays the primary role for designing the vector fields $e_1, e_2$, we assume for simplicity of description in this work that $e_1, e_2$ depend only on the geometry of the surface and thus remain fixed. Note here that "anisotropic" means that the flux of the PDE may not be parallel to $\nabla_{\mathcal{M}} u$.

**4. Discrete filtering over triangulated surfaces.** In this section we derive our discrete filtering schemes on triangulated mesh surfaces according to the diffusion equations (3.7), (3.8), and (3.9). The schemes include linear filtering, nonlinear filtering, and anisotropic filtering.

Given $M$ as a triangulated mesh approximation to the manifold $\mathcal{M}$, we use notation introduced in section 2 in the following. Under this discrete setting, the functions $u = u(p)$ and $f = f(p)$ are understood as piecewise linear functions. We also assume as in [61] that $e_1(p), e_2(p)$ of the anisotropic diffusion equation (3.9) are two orthonormal piecewise constant vector fields in the tangent space of $M$ (see subsection 4.1). That is, $e_1(p)$ and $e_2(p)$ are constant vectors in each triangle of $M$ and constitute an orthonormal basis of the underlying space of the triangle.

We first define the tangent space, integration, and differential operators on $M$.

**4.1. Integration, gradient, and divergence on triangulated surfaces.** $M$ has a natural piecewise parametrization $\{U_{\tau_i} = (\xi^1_{\tau_i}, \xi^2_{\tau_i}), \tau_i\}_{0 \le i \le \mathrm{T}-1}$, in which each $U_{\tau_i}$ has a flat Riemannian metric; i.e., $(\xi^1_{\tau_i}, \xi^2_{\tau_i})$ is a Cartesian coordinate. For a point $p \in \mathrm{Interior}(\tau_i)$, the tangent space is nothing but the triangle $\tau_i$ and has a basis $\{\frac{\partial}{\partial \xi^1_{\tau_i}}, \frac{\partial}{\partial \xi^2_{\tau_i}}\}$. For other points located on edges of the triangle mesh $M$, the tangent space can be defined using interpolation techniques, which will be reported together with the related geometry in a future work. Here we just omit it since we do not use these tangent spaces in this paper. It should be pointed out that the choice of the local coordinate $(\xi^1_{\tau_i}, \xi^2_{\tau_i})$ is flexible, depending on the convenience of the computation.

The integral of a function $f$ on $M$ reads as follows:

$$\int_M f(p)dM = \sum_{0 \le i \le \mathrm{T}-1} \int_{U_{\tau_i}} f(p)\sqrt{\mathbf{g}}d\xi^1_{\tau_i}d\xi^2_{\tau_i} = \sum_{\tau} \int_{\tau} f(p)d\tau, \tag{4.1}$$

where $\mathbf{g}$ is the metric tensor determined by the local parametrization. By noticing the tetra-

hedron of the graph of $\phi_i$ over the triangle, we have

$$\int_M f(p)dM = \sum_{\tau=[v_i,v_j,v_k]} \frac{s_\tau}{3}(f_i+f_j+f_k) = \sum_{0\le i\le \mathrm{V}-1} f_i \sum_{\tau\in D_1(i)} \frac{s_\tau}{3} = \sum_{0\le i\le \mathrm{V}-1} f_i s_i, \tag{4.2}$$

where $s_\tau$ is the area of the triangle $\tau$, and $s_i$ is the area of the control cell of the vertex $v_i$. We also have the integration of $f$ along a curve $N \subset M$:

$$\int_N f(p)dN = \sum_{0\le i\le \mathrm{T}-1} \int_{V_{\tau_i}} f(p(\eta)) \left|\frac{\partial p}{\partial \eta}\right| d\eta = \sum_\tau \int_{\tau \bigcap N} f(p)dN, \tag{4.3}$$

where $\{V_{\tau_i}, \tau_i \bigcap N\}_{0\le i\le \mathrm{T}-1}$ is the local parametrization of $N$.

We now define the gradient operator $\nabla_M$ on $M$. Given the piecewise linear function $u = u(p) = \sum_j u_j\phi_j(p)$, its gradient is as follows:

$$\nabla_M u(p) = \sum_j u_j \nabla_M \phi_j(p), \tag{4.4}$$

where $\nabla_M\phi_j(p)$ will be calculated using the natural piecewise parametrization; see Figure 2(a). Since $\phi_j(p)$ is linear in $\tau$ with $\phi_j(v_j) = 1$ and $\phi_j(v_i) = \phi_j(v_k) = 0$, we choose the local coordinate $(\xi_\tau^1, \xi_\tau^2)$ as shown in the figure. We assume the mapping from the local coordinate to $\tau$ is

$$p = v_i + \xi_\tau^1(v_k - v_i) + \xi_\tau^2(v_j - O),$$

where $O$ is the Euclidean projection of $v_j$ on the line passing through $v_i, v_k$. Then we deduce

$$\mathbf{g} = \begin{pmatrix} (v_k-v_i)\cdot(v_k-v_i) & 0 \\ 0 & (v_j-O)\cdot(v_j-O) \end{pmatrix},$$

and $\frac{\partial\phi_j}{\partial\xi_\tau^1} = 0$, $\frac{\partial\phi_j}{\partial\xi_\tau^2} = 1$, yielding

$$\nabla_M\phi_j = \frac{v_j - O}{|v_j - O|^2}, \tag{4.5}$$

according to (3.4); see the red vector in Figure 2(a). As one can see, $\nabla_M\phi_j$ is a piecewise constant vector, and thus so is $\nabla_M u$.

Given a vector field $X \in TM$, one can similarly calculate the divergence $(\mathrm{div}_M X)(p)$ for $p \in \mathrm{Interior}(\tau)$ for some $\tau$ according to (3.5) using local coordinates. However, here we are more interested in the divergence at vertices of $M$, e.g., $(\mathrm{div}_M X)(v_i)$, since in applications the functions in the diffusion equations (3.7), (3.8), and (3.9) are usually given by assigning values on vertices. For vertex $v_i$, we approximate $(\mathrm{div}_M X)(v_i)$ by the average of the divergence in the control cell $C_i$ as

$$(\mathrm{div}_M X)(v_i) = \frac{1}{s_i}\int_{C_i} \mathrm{div}_M X dC_i.$$

By the divergence theorem (see (3.6)) and (2.1), (2.2), we have

$$(\mathrm{div}_M X)(v_i) = \frac{1}{s_i} \sum_{\tau\in D_1(i)} \int_{\bigcup\limits_{v_i\prec e\prec\tau} [BC(e), BC(\tau)]} X\cdot\vec{n} d\partial C_i \tag{4.6}$$

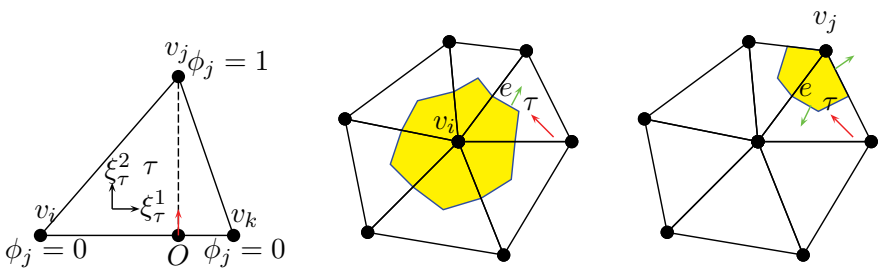


(a) $\nabla_M \phi_j$ restricted in $\tau$ (b) $(\mathrm{div}_M X)_{v_i}$ (c) $(\mathrm{div}_M X)_{v_j}$

**Figure 2.** *Gradient and divergence.* (a) *The gradient of the basis $\phi_j$ restricted in $\tau$: the red vector.* (b) *The divergence of a vector field $X$ at an interior vertex $v_i$: the red vector is $X$ restricted in $\tau$; the green vector is the outward normal of $[BC(e), BC(\tau)] \subset \partial C_i$.* (c) *The divergence of a vector field $X$ at a boundary vertex $v_j$: the red vector is $X$ restricted in $\tau$; the green vector is the outward normal of $[BC(e), BC(\tau)] \subset \partial C_j$ or $[BC(v_j), BC(e)] \subset \partial C_j$.*

for an interior vertex $v_i$, and

$$(\mathrm{div}_M X)(v_j) = \frac{1}{s_j}\left( \sum_{\tau \in D_1(j)} \int_{\bigcup_{v_j \prec e \prec \tau} [BC(e), BC(\tau)]} X \cdot \vec{n} d\partial C_j + \sum_{v_j \prec e \subset \partial M} \int_{[BC(v_j), BC(e)]} X \cdot \vec{n} d\partial C_j \right) \tag{4.7}$$

for a boundary vertex $v_j$, where $\vec{n}$ is the outward normal of $\partial C_i$ or $\partial C_j$; see Figures 2(b) and 2(c).

**4.2. Discrete filtering on triangulated surfaces.** We can now discretize the diffusion equations (3.7), (3.8), and (3.9) via approximating the equations at vertices with the differential operators defined above, to construct our discrete filtering procedures. The derivation is equivalent to FVM discretization in [61].

It should be pointed out that one can also find a parametric or implicit representation of the triangulated surface and then use the methods as in [22] or [5] to solve the problem. There are several issues [61] to be considered in these two approaches. First, the additive operator splitting (AOS) method [25, 39] as a very fast method for problems on regular grids can be used in the piecewise parametrization-based method. Also the problem will be solved in a narrow band near the surface if one first implicitizes the triangular mesh and then uses the level-set method [5]. Second, in many applications the data are given and should be maintained after calculations as a triangular mesh. This requires transformations of surface and image data between triangular meshes and parametric or implicit representations. These transformations are usually difficult and expensive. Meshes with complex topology such as high genus are very difficult to parametrize. Besides, the parametrization always brings metric distortions [50]. It is also not straightforward to transform the image data defined on the triangular mesh to the parametric domains (for a parametrization-based method) or 3-dimensional (3D) grids (for a level–set-based method). In the parametrization-based method, whether AOS schemes are

used or not, one needs to interpolate the data defined on vertices of the mesh and then resample the interpolation function on regular grids of the parametric domains. In the level–set-based method, the transformation of the image data from the triangular mesh to the 3D grids is actually an inverse procedure of data interpolation plus a data extension operation [5]. The inverse interpolation is not easy or accurate if the grids are too sparse. Also the data extension (usually based on a PDE) costs CPU time. The third issue is that many triangular meshes in applications are feature adaptive, and thus the triangles are irregular and nonuniform. This brings errors and extra memory requirements for parametric and implicit representations.

**4.2.1. Discrete linear filtering.** We approximate the linear heat equation (3.7) at each vertex of $M$. For an interior vertex $v_i$,

$$(u_t)(v_i) = (\mathrm{div}_M \nabla_M u)(v_i) = \frac{1}{s_i} \sum_{\tau \in D_1(i)} \int_{\bigcup\limits_{v_i \prec e \prec \tau} [BC(e), BC(\tau)]} \nabla_M u \cdot \vec{n} d\partial C_i, \tag{4.8}$$

according to (4.6). Since $\nabla_M u$ is a constant when restricted in $\tau$, the right-hand side of (4.8) is actually

$$\frac{1}{s_i} \sum_{\tau \in D_1(i)} \nabla_M u \cdot \int_{\bigcup\limits_{v_i \prec e \prec \tau} [BC(e), BC(\tau)]} \vec{n} d\partial C_i.$$

By exchanging the order of sums, we obtain

$$(\mathrm{div}_M \nabla_M u)(v_i) = \frac{1}{s_i} \left( u_i \omega_{ii} + \sum_{j \in N_1(i)} u_j \omega_{ij} \right), \tag{4.9}$$

where

$$\begin{cases} \omega_{ij} = \displaystyle\sum_{\tau, [v_i, v_j] \prec \tau} \nabla_M \phi_j \cdot \int_{\bigcup\limits_{e, v_i \prec e \prec \tau} [BC(e), BC(\tau)]} \vec{n} dl, \\ \omega_{ii} = - \displaystyle\sum_{j \in N_1(i)} \omega_{ij}. \end{cases} \tag{4.10}$$

If $v_i$ is a boundary vertex, by a similar derivation, we get the same expression as (4.9) by noticing the boundary condition of PDE (3.7). Thus (4.9) is a uniform spatial discretization for all meshes (with or without boundaries).

We then have the following implicit discretization:

$$\frac{u_i^{n+1} - u_i^n}{\triangle t} = \frac{1}{s_i} \left( u_i^{n+1} \omega_{ii} + \sum_{j \in N_1(i)} u_j^{n+1} \omega_{ij} \right). \tag{4.11}$$

Denoting $u^{(n)} = (u_0^n, u_1^n, \ldots, u_{\mathrm{V}-1}^n)^T$, (4.11) is formulated into the following matrix form:

$$(S + \triangle t W) u^{(n+1)} = S u^{(n)}, \tag{4.12}$$

where $S = \mathrm{diag}(s_0, s_1, \ldots, s_{\mathrm{V}-1})$ and $W = (-\omega_{ij})_{\mathrm{V}\times\mathrm{V}}$. $W$ is a highly sparse and symmetric matrix since

$$\omega_{ij} = \frac{1}{2}(\cot\alpha_{ij} + \cot\beta_{ij}) = \omega_{ji}, j \in N_1(i). \tag{4.13}$$

See Figure 3(b) for an illustration and the remarks on computational details in section 4.2.4.

**4.2.2. Discrete nonlinear filtering.** As for the nonlinear diffusion equation (3.8), a derivation similar to that of the linear equation can be made. Concretely, we have

$$(u_t)(v_i) = (\mathrm{div}_M(g(|\nabla_M u|)\nabla_M u))(v_i). \tag{4.14}$$

By the boundary condition of (3.8), the right-hand side of (4.14) is

$$\frac{1}{s_i}\sum_{\tau\in D_1(i)}\int_{\bigcup_{v_i\prec e\prec\tau}[BC(e),BC(\tau)]} g(|\nabla_M u|)\nabla_M u\cdot\vec{n}d\partial C_i$$

for any (interior or boundary) vertex $v_i$. Using the fact that $\nabla_M u$ is a constant in $\tau$, we further deduce

$$(\mathrm{div}_M(g(|\nabla_M u|)\nabla_M u))(v_i) = \frac{1}{s_i}\sum_{\tau\in D_1(i)} g(|\nabla_M u|)\nabla_M u\cdot\int_{\bigcup_{v_i\prec e\prec\tau}[BC(e),BC(\tau)]}\vec{n}d\partial C_i.$$

The contribution of triangle $\tau = [v_i, v_j, v_k]$ in the summation of the above equation is

$$g(|\nabla_M u|_\tau|)(u_i c_{ii,\tau} + u_j c_{ij,\tau} + u_k c_{ik,\tau}),$$

where

$$\begin{cases} c_{ij,\tau} = \nabla_M\phi_j\cdot\displaystyle\int_{\bigcup_{e,v_i\prec e\prec\tau}[BC(e),BC(\tau)]}\vec{n}dl, \\ c_{ik,\tau} = \nabla_M\phi_k\cdot\displaystyle\int_{\bigcup_{e,v_i\prec e\prec\tau}[BC(e),BC(\tau)]}\vec{n}dl, \\ c_{ii,\tau} = -c_{ij,\tau} - c_{ik,\tau}. \end{cases} \tag{4.15}$$

We then come to the semi-implicit discretization of (3.8) as

$$\frac{u_i^{n+1}-u_i^n}{\triangle t} = \frac{1}{s_i}\sum_{\tau=[v_i,v_j,v_k]\in D_1(i)} g(|\nabla_M u|_\tau^n|)(u_i^{n+1}c_{ii,\tau} + u_j^{n+1}c_{ij,\tau} + u_k^{n+1}c_{ik,\tau}),$$

which can be written in matrix form:

$$(S + \triangle t H(u^{(n)}))u^{(n+1)} = Su^{(n)}, \tag{4.16}$$

where $S$ and $u^{(n)}$ are defined above and $H(u^{(n)}) = (-h_{ij})_{\mathrm{V}\times\mathrm{V}}$ with

$$h_{ij} = \begin{cases} \displaystyle\sum_{\tau,[v_i,v_j]\prec\tau} g(|\nabla_M u|_\tau^n|)c_{ij,\tau}, & j \in N_1(i), \\ \displaystyle\sum_{\tau\in D_1(i)} g(|\nabla_M u|_\tau^n|)c_{ii,\tau}, & j = i, \\ 0 & \text{otherwise.} \end{cases} \tag{4.17}$$

$H$ is also highly sparse and symmetric since

$$c_{ij,\tau} = \frac{1}{2}\cot\alpha_{ij} = c_{ji,\tau}. \tag{4.18}$$

See Figure 3(b) and the remarks in section 4.2.4.

**4.2.3. Discrete anisotropic filtering.** Similarly, we approximate the anisotropic diffusion equation (3.9) as

$$(u_t)(v_i) = (\mathrm{div}_M(g_1(|\nabla_M u|)(\nabla_M u\cdot e_1)e_1 + g_2(|\nabla_M u|)(\nabla_M u\cdot e_2)e_2))(v_i). \tag{4.19}$$

According to the boundary condition of (3.9), we have a uniform expression for the right-hand side of (4.19) as

$$\frac{1}{s_i}\sum_{\tau\in D_1(i)}\int_{\bigcup\limits_{v_i\prec e\prec\tau}[BC(e),BC(\tau)]}(g_1(|\nabla_M u|)(\nabla_M u\cdot e_1)e_1 + g_2(|\nabla_M u|)(\nabla_M u\cdot e_2)e_2)\cdot\vec{n}d\partial C_i$$

for all vertices, which can be reformulated into

$$\frac{1}{s_i}\sum_{\tau\in D_1(i)}(g_1(|\nabla_M u|)(\nabla_M u\cdot e_1)e_1 + g_2(|\nabla_M u|)(\nabla_M u\cdot e_2)e_2)\cdot\int_{\bigcup\limits_{v_i\prec e\prec\tau}[BC(e),BC(\tau)]}\vec{n}d\partial C_i,$$

since $g_1, g_2, \nabla_M u, e_1, e_2$ are all constant in triangle $\tau$. Concretely, the contribution of triangle $\tau = [v_i, v_j, v_k]$ in the above summation is

$$g_1(|\nabla_M u|_\tau|)(u_i c^1_{ii,\tau} + u_j c^1_{ij,\tau} + u_k c^1_{ik,\tau}) + g_2(|\nabla_M u|_\tau|)(u_i c^2_{ii,\tau} + u_j c^2_{ij,\tau} + u_k c^2_{ik,\tau}),$$

where

$$\begin{cases} c^1_{ij,\tau} = (\nabla_M\phi_j\cdot e_1)\left(e_1\cdot\displaystyle\int_{\bigcup\limits_{e,v_i\prec e\prec\tau}[BC(e),BC(\tau)]}\vec{n}dl\right), \\ c^2_{ij,\tau} = (\nabla_M\phi_j\cdot e_2)\left(e_2\cdot\displaystyle\int_{\bigcup\limits_{e,v_i\prec e\prec\tau}[BC(e),BC(\tau)]}\vec{n}dl\right), \\ c^1_{ik,\tau} = (\nabla_M\phi_k\cdot e_1)\left(e_1\cdot\displaystyle\int_{\bigcup\limits_{e,v_i\prec e\prec\tau}[BC(e),BC(\tau)]}\vec{n}dl\right), \\ c^2_{ik,\tau} = (\nabla_M\phi_k\cdot e_2)\left(e_2\cdot\displaystyle\int_{\bigcup\limits_{e,v_i\prec e\prec\tau}[BC(e),BC(\tau)]}\vec{n}dl\right), \\ c^1_{ii,\tau} = -c^1_{ij,\tau} - c^1_{ik,\tau}, \quad c^2_{ii,\tau} = -c^2_{ij,\tau} - c^2_{ik,\tau}. \end{cases} \tag{4.20}$$

Therefore, the semi-implicit scheme of the anisotropic equation (3.9) is

$$\frac{u_i^{n+1}-u_i^n}{\triangle t}=\frac{1}{s_i}\Bigg(\sum_{\tau\in D_1(i)} g_1(|\nabla_M u|_\tau^n|)(u_i^{n+1}c_{ii,\tau}^1+u_j^{n+1}c_{ij,\tau}^1+u_k^{n+1}c_{ik,\tau}^1) + \sum_{\tau\in D_1(i)} g_2(|\nabla_M u|_\tau^n|)(u_i^{n+1}c_{ii,\tau}^2+u_j^{n+1}c_{ij,\tau}^2+u_k^{n+1}c_{ik,\tau}^2)\Bigg)$$

or, in matrix form,

$$(S+\triangle t L(u^{(n)}))u^{(n+1)}=Su^{(n)}, \tag{4.21}$$

where $L(u^{(n)})=(-l_{ij})_{\mathrm{V}\times\mathrm{V}}$ with

$$l_{ij}=\begin{cases}\displaystyle\sum_{\tau,[v_i,v_j]\prec\tau}(g_1(|\nabla_M u|_\tau^n|)c_{ij,\tau}^1+g_2(|\nabla_M u|_\tau^n|)c_{ij,\tau}^2), & j\in N_1(i),\\ \displaystyle\sum_{\tau\in D_1(i)}(g_1(|\nabla_M u|_\tau^n|)c_{ii,\tau}^1+g_2(|\nabla_M u|_\tau^n|)c_{ii,\tau}^2), & j=i,\\ 0 & \text{otherwise.}\end{cases} \tag{4.22}$$

Similarly, $L$ is also highly sparse and symmetric since

$$\begin{cases} c_{ij,\tau}^1=\frac{1}{2\sin\angle k}\cos\theta\cos(\theta-\angle k)=c_{ji,\tau}^1,\\ c_{ij,\tau}^2=\frac{1}{2\sin\angle k}\sin\theta\sin(\theta-\angle k)=c_{ji,\tau}^2\end{cases} \tag{4.23}$$

as obtained in [61]; see Figures 3(c) and (d) and the following subsection. Here the angle $\angle k$ is with respect to the vertex $v_k$ of $\tau$.

**4.2.4. Some computational details.** In this subsection we give some remarks on computing those coefficients defined in (4.10), (4.15), and (4.20), as well as solving the linear systems (4.12), (4.16), and (4.21).

As one can see, the integrals of the normal vectors over the boundaries of control cells play an important role. We present here the following theorem from [61].

Theorem 4.1. *Let $\tau=[A,B,C]$ be a triangle and $\Gamma=\Gamma(t)$, $t\in[0,1]$, be an arbitrary curve within the triangle with endpoints $\Gamma(0)=P$ and $\Gamma(1)=Q$ as shown in Figure 3(a); then*

$$\int_{\Gamma(t)}\vec{n}dl=|PQ|\vec{n}_{PQ}, \tag{4.24}$$

*where $\vec{n}$ is the normal vector of $\Gamma(t)$ and $\vec{n}_{PQ}$ is the unit vector perpendicular to the line segment $[P,Q]=\Gamma(1)-\Gamma(0)$.*

According to Theorem 4.1 and the gradient $\nabla_M\phi_j$ in (4.5), one can use basic vector calculus to obtain the expressions in (4.13), (4.18), and (4.23); see Figure 3.

The highly sparse systems (4.12), (4.16), and (4.21) can be solved by the preconditioned biconjugate gradient method. There $H(u^{(n)})$ in (4.16) and $L(u^{(n)})$ in (4.21) depend not only on the coefficients $\{c_{ii,\tau},c_{ij,\tau},c_{ik,\tau},c_{ji,\tau},c_{jj,\tau},c_{jk,\tau},c_{ki,\tau},c_{kj,\tau},c_{kk,\tau},c_{ii,\tau}^1,c_{ij,\tau}^1,c_{ik,\tau}^1,c_{ii,\tau}^2,c_{ij,\tau}^2,c_{ik,\tau}^2,$

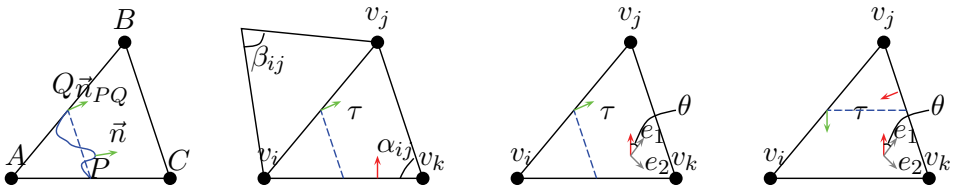


(a) normal vector integral (b) $\omega_{ij}$ and $c_{ij,\tau}$ (c) $c^1_{ij,\tau}$ and $c^2_{ij,\tau}$ (d) $c^1_{ji,\tau}$ and $c^2_{ji,\tau}$

**Figure 3.** (a) *The integral of the normal vector of a curve in* $\tau$. (b), (c), (d) *Computation of* $\omega_{ij}, c_{ij,\tau}$, $c^1_{ij,\tau}, c^2_{ij,\tau}, c^1_{ji,\tau}, c^2_{ji,\tau}$. *The dotted blue lines, the green arrows, and the red arrows stand for the integrals of the boundaries of the control cells in* $\tau$, *outer normal directions of blue lines, and gradients of the basis such as* $\phi_i$, $\phi_j$, *respectively.* $\theta$ *is the clockwise rotation from* $\nabla_M \phi_j$ *to* $e_1$.

$c^1_{ji,\tau}, c^1_{jj,\tau}, c^1_{jk,\tau}, c^2_{ji,\tau}, c^2_{jj,\tau}, c^2_{jk,\tau}, c^1_{ki,\tau}, c^1_{kj,\tau}, c^1_{kk,\tau}, c^2_{ki,\tau}, c^2_{kj,\tau}, c^2_{kk,\tau}\}$, but also on the data $u^{(n)}$. Hence they should be updated dynamically. Fortunately, the updating procedure is very simple and does not require much CPU time due to their sparseness and inherent sophisticated storage structure from the data structure of the mesh surfaces. Since we are focusing on the analysis in this paper, the reader is referred to the appendix of [61] for the implementation details.

## 5. Scale-space analysis of discrete filtering.

In this section, we analyze the three types of discrete filtering using scale-space concepts. For convenience of description, we first construct three discrete scale-spaces corresponding to the filtering procedures.

### 5.1. From discrete filtering to discrete scale-spaces.

Each discrete filtering procedure gives a discrete scale-space.

#### 5.1.1. Linear scale-space.

Let $f$ be a given image. From (4.12), with a fixed time step, one calculates a sequence of images $\{u^{(n)}, n = 0, 1, 2, \ldots\}$ as follows:

$$\begin{cases} u^{(0)} = f, \\ (S + \triangle t W) u^{(n+1)} = S u^{(n)}. \end{cases} \tag{5.1}$$

We call the image sequence $\{T_n^{LD} f = u^{(n)}, n = 0, 1, 2, \ldots\}$ the *discrete linear scale-space* of $f$, and $n$ is the discrete scale.

#### 5.1.2. Nonlinear scale-space.

Let $f$ be a given image. With a fixed time step, the image sequence $\{T_n^{ND} f = u^{(n)}, n = 0, 1, 2, \ldots\}$ calculated from

$$\begin{cases} u^{(0)} = f, \\ (S + \triangle t H(u^{(n)})) u^{(n+1)} = S u^{(n)} \end{cases} \tag{5.2}$$

is called the *discrete nonlinear scale-space* of $f$, and $n$ is the discrete scale.

#### 5.1.3. Anisotropic scale-space.

Assume that $f$ is a given image. The image sequence $\{T_n^{AD} f = u^{(n)}, n = 0, 1, 2, \ldots\}$ calculated from

$$\begin{cases} u^{(0)} = f, \\ (S + \triangle t L(u^{(n)})) u^{(n+1)} = S u^{(n)} \end{cases} \tag{5.3}$$

is called the *discrete anisotropic scale-space* of $f$, and $n$ is the discrete scale.

**5.2. Scale-space analysis.** In this subsection, we discuss several properties of the discrete filtering procedures by analyzing the image sequences of the discrete scale-spaces. These properties include existence and uniqueness, continuous dependence on initial value, grey level shift invariance, the discrete semigroup property, information reduction, and constant limit behavior.

**5.2.1. Existence, uniqueness, and continuous dependence on initial value.** We first analyze the matrices $W, H(u^{(n)}), L(u^{(n)})$ in (5.1), (5.2), and (5.3).

Theorem 5.1. *Let $v$ be any vector and $v(p)$ be the piecewise linear function interpolating vertex data $v$ on $M$.*

(1) *The matrix $W$ in (5.1) is symmetric, and*

$$v'Wv = \int_M |\nabla_M v(p)|^2 dM. \tag{5.4}$$

*Therefore $W$ is positive semidefinite with* $\operatorname{rank}(W) = \mathrm{V} - 1$.

(2) *$H(u^{(n)})$ in (5.2) is also symmetric, and*

$$v'H(u^{(n)})v = \sum_\tau g(|\nabla_M u|_\tau^n|) \int_\tau |\nabla_M v(p)|^2 d\tau. \tag{5.5}$$

*Therefore $H(u^{(n)})$ is positive semidefinite. Furthermore,* $\operatorname{rank}(H(u^{(n)})) = \mathrm{V} - 1$ *when $g(\cdot) > 0$.*

(3) *$L(u^{(n)})$ in (5.3) is symmetric, and*

$$v'L(u^{(n)})v = \sum_\tau \left( g_1^n|_\tau \int_\tau (\nabla_M v(p) \cdot e_1)^2 d\tau + g_2^n|_\tau \int_\tau (\nabla_M v(p) \cdot e_2)^2 d\tau \right), \tag{5.6}$$

*where $g_1^n|_\tau = g_1(|\nabla_M u|_\tau^n|)$ and $g_2^n|_\tau = g_2(|\nabla_M u|_\tau^n|)$. Hence $L(u^{(n)})$ is positive semidefinite. Furthermore,* $\operatorname{rank}(L(u^{(n)})) = \mathrm{V} - 1$ *when $g_1(\cdot) > 0$, $g_2(\cdot) > 0$.*

*Proof.* (1) The symmetry of $W$ is obvious since $\omega_{ij} = \omega_{ji}$. On the other hand, for any vector $v$,

$$\begin{aligned}
v'Wv &= \sum_{i,j}(-\omega_{ij}v_iv_j) = -\sum_i \omega_{ii}v_i^2 - \sum_i \sum_{j\in N_1(i)} \omega_{ij}v_iv_j \\
&= \sum_i \sum_{j\in N_1(i)} \omega_{ij}v_i^2 - \sum_i \sum_{j\in N_1(i)} \omega_{ij}v_iv_j \\
&= \sum_{e=[v_i,v_j]} \omega_{ij}(v_i^2 + v_j^2) - \sum_{e=[v_i,v_j]} 2\omega_{ij}v_iv_j = \sum_{e=[v_i,v_j]} \omega_{ij}(v_i - v_j)^2 \\
&= \frac{1}{2} \sum_{\tau=[v_i,v_j,v_k]} (\cot\theta_i(v_j - v_k)^2 + \cot\theta_j(v_i - v_k)^2 + \cot\theta_k(v_i - v_j)^2) \\
&= \sum_{\tau=[v_i,v_j,v_k]} \int_\tau |\nabla_M v(p)|^2 dM = \int_M |\nabla_M v(p)|^2 dM \geq 0,
\end{aligned}$$

where $v(p)$ is the piecewise linear function interpolating vertex data $v$. Here we recall

$$\nabla_M v(p)|_{\tau=[v_i,v_j,v_k]} = v_i\nabla_M\phi_i + v_j\nabla_M\phi_j + v_k\nabla_M\phi_k$$

and the gradient in (4.5). Hence $W$ is positive semidefinite. Moreover, $v'Wv = 0$ if and only if $v = c\ (1, 1, \ldots, 1)$ with constant $c$. This shows $\text{rank}(W) = \text{V} - 1$.

(2) $H(u^{(n)})$ is symmetric since $c_{ij,\tau} = c_{ji,\tau}$. On the other hand, for any vector $v$,

$$\begin{aligned}
v'H(u^{(n)})v &= \sum_{ij}(-h_{ij}v_iv_j) = -\sum_i h_{ii}v_i^2 - \sum_i\sum_{j\in N_1(i)} h_{ij}v_iv_j \\
&= -\sum_i\sum_{\tau,\tau\in D_1(i)} g(|\nabla_M u|_\tau^n|)c_{ii,\tau}v_i^2 - \sum_i\sum_{j\in N_1(i)}\sum_{\tau,[v_i,v_j]\prec\tau} g(|\nabla_M u|_\tau^n|)c_{ij,\tau}v_iv_j \\
&= \sum_{e=[v_i,v_j]}\sum_{\tau,e\prec\tau} g(|\nabla_M u|_\tau^n|)c_{ij,\tau}(v_i^2+v_j^2) - \sum_{e=[v_i,v_j]}\sum_{\tau,e\prec\tau} g(|\nabla_M u|_\tau^n|)c_{ij,\tau}2v_iv_j \\
&= \sum_{e=[v_i,v_j]}\sum_{\tau,e\prec\tau} g(|\nabla_M u|_\tau^n|)c_{ij,\tau}(v_i-v_j)^2 \\
&= \sum_{\tau=[v_i,v_j,v_k]} g(|\nabla_M u|_\tau^n|)(c_{ij,\tau}(v_i-v_j)^2 + c_{ik,\tau}(v_i-v_k)^2 + c_{jk,\tau}(v_j-v_k)^2) \\
&= \sum_{\tau=[v_i,v_j,v_k]} g(|\nabla_M u|_\tau^n|)\frac{1}{2}(\cot\theta_k(v_i-v_j)^2 + \cot\theta_j(v_i-v_k)^2 + \cot\theta_i(v_j-v_k)^2) \\
&= \sum_{\tau=[v_i,v_j,v_k]} g(|\nabla_M u|_\tau^n|)\int_\tau |\nabla_M v(p)|^2 d\tau \geq 0,
\end{aligned}$$

where we thank the fact that $|\nabla_M u|_\tau^n|$ is constant for each $\tau$. This gives the semidefinite positiveness of $H(u^{(n)})$. The reason for $\text{rank}(H(u^{(n)})) = \text{V} - 1$ when $g(\cdot) > 0$ is the same as (1).

(3) The symmetry of $L(u^{(n)})$ follows from the fact that $c^1_{ij,\tau} = c^1_{ji,\tau}$ and $c^2_{ij,\tau} = c^2_{ji,\tau}$. For any $v$,

$$\begin{aligned}
v'L(u^{(n)})v &= \sum_{ij}(-l_{ij}v_iv_j) = -\sum_i l_{ii}v_i^2 - \sum_i\sum_{j\in N_1(i)} l_{ij}v_iv_j \\
&= -\sum_i\sum_{\tau,\tau\in D_1(i)} (g_1^n|_\tau c^1_{ii,\tau} + g_2^n|_\tau c^2_{ii,\tau})v_i^2 - \sum_i\sum_{j\in N_1(i)}\sum_{\tau,[v_i,v_j]\prec\tau} (g_1^n|_\tau c^1_{ij,\tau} + g_2^n|_\tau c^2_{ij,\tau})v_iv_j \\
&= \sum_{e=[v_i,v_j]}\sum_{\tau,e\prec\tau} (g_1^n|_\tau c^1_{ij,\tau} + g_2^n|_\tau c^2_{ij,\tau})(v_i^2+v_j^2) - \sum_{e=[v_i,v_j]}\sum_{\tau,e\prec\tau} (g_1^n|_\tau c^1_{ij,\tau} + g_2^n|_\tau c^2_{ij,\tau})2v_iv_j \\
&= \sum_{e=[v_i,v_j]}\sum_{\tau,e\prec\tau} (g_1^n|_\tau c^1_{ij,\tau} + g_2^n|_\tau c^2_{ij,\tau})(v_i-v_j)^2 \\
&= \sum_{\tau=[v_i,v_j,v_k]} g_1^n|_\tau(c^1_{ij,\tau}(v_i-v_j)^2 + c^1_{ik,\tau}(v_i-v_k)^2 + c^1_{jk,\tau}(v_j-v_k)^2) \\
&\quad + \sum_{\tau=[v_i,v_j,v_k]} g_2^n|_\tau(c^2_{ij,\tau}(v_i-v_j)^2 + c^2_{ik,\tau}(v_i-v_k)^2 + c^2_{jk,\tau}(v_j-v_k)^2)
\end{aligned}$$

$$= \sum_{\tau=[v_i,v_j,v_k]} \left( g_1^n|_\tau \int_\tau (\nabla_M v(p) \cdot e_1)^2 d\tau + g_2^n|_\tau \int_\tau (\nabla_M v(p) \cdot e_2)^2 d\tau \right) \geq 0,$$

where the last equality can be verified via vector operations and formulas of trigonometric functions. This gives the semidefinite positiveness of $L(u^{(n)})$. Similarly, $v'Lv = 0$ if and only if $v = c\ (1, 1, \ldots, 1)$ with constant $c$, which shows $\text{rank}(L(u^{(n)})) = \text{V} - 1$ when $g_1(\cdot) > 0$, $g_2(\cdot) > 0$. ■

We can now prove the following theorem.

Theorem 5.2. *Given an initial image $f$, after choosing a time step $\triangle t$, there exist a unique discrete linear scale-space $\{T_n^{LD} f = u^{(n)},\ n = 0, 1, 2, \ldots\}$, a unique discrete nonlinear scale-space $\{T_n^{ND} f = u^{(n)}, n = 0, 1, 2, \ldots\}$ and a unique discrete anisotropic scale-space $\{T_n^{AD} f = u^{(n)},\ n = 0, 1, 2, \ldots\}$ which depend continuously on the initial image $f$ for every finite $n$.*

*Proof.* We need only prove that the coefficient matrices in (5.1), (5.2), and (5.3) are invertible.

The invertibility of $S + \triangle t W$, $(S + \triangle t H(u^{(n)}))$, and $(S + \triangle t L(u^{(n)}))$ is obvious since $S$ is positive definite, and $W, H(u^{(n)}), L(u^{(n)})$ are all positive semidefinite. The continuous dependence follows from the continuity of $W, H(u^{(n)}), L(u^{(n)})$. ■

**5.2.2. Discrete semigroup property.** The discrete scale-spaces satisfy the following discrete semigroup property.

Proposition 5.3. *For any $n_1 \geq 0$ and $n_2 \geq 0$,*

(1) $T_{n_1+n_2}^{LD} f = T_{n_2}^{LD}(T_{n_1}^{LD} f) = T_{n_1}^{LD}(T_{n_2}^{LD} f)$;

(2) $T_{n_1+n_2}^{ND} f = T_{n_2}^{ND}(T_{n_1}^{ND} f) = T_{n_1}^{ND}(T_{n_2}^{ND} f)$;

(3) $T_{n_1+n_2}^{AD} f = T_{n_2}^{AD}(T_{n_1}^{AD} f) = T_{n_1}^{AD}(T_{n_2}^{AD} f)$.

*Proof.* The proof is by direct verification. ■

**5.2.3. Grey level shift invariance.** The discrete scale-spaces all have the grey level shift invariance property.

Proposition 5.4. *Let $C = (c, c, \ldots, c)$ be a V-dimensional vector. Then the discrete scale-spaces satisfy*

(1) $T_n^{LD}(f + C) = T_n^{LD}(f) + C$;

(2) $T_n^{ND}(f + C) = T_n^{ND}(f) + C$;

(3) $T_n^{AD}(f + C) = T_n^{AD}(f) + C$.

*Proof.* We prove only (1) (the proofs of (2) and (3) are similar). First, we show that (1) holds for $n = 1$.

If we can show

$$(S + \triangle t W)(T_1^{LD}(f) + C) = S(f + C),$$

then (1) holds by the uniqueness of the discrete linear scale-space. Since

$$(S + \triangle t W) T_1^{LD}(f) = Sf,$$

we need only prove

$$(S + \triangle t W) C = SC,$$

which is true since the sum of each row of $W$ vanishes.

For general $n$, (1) follows from the discrete semigroup property. ∎

**5.2.4. Reverse contrast invariance.** Since $W$ is independent of $u$, $H(-u) = H(u)$, and $L(-u) = L(u)$, we have the following proposition.

Proposition 5.5. *Let $f$ be an initial image. Then*

(1) $T_n^{LD}(-f) = -T_n^{LD} f$;

(2) $T_n^{ND}(-f) = -T_n^{ND} f$;

(3) $T_n^{AD}(-f) = -T_n^{AD} f$.

**5.2.5. Conservation of total grey level.** We define the total grey level of a function $u$ on a triangulated surface as its integral. That is,

$$\mu(u) = \int_M u(p)dM = \sum_{i=0,1,\ldots,\mathrm{V}-1} u_i s_i, \tag{5.7}$$

according to (4.2), where $s_i$ is the area of the control cell of the vertex $v_i$.

Proposition 5.6. *The total grey level $\mu(f)$ does not change in the discrete scale-spaces; that is,*

$$\mu(T_n^{LD} f) = \mu(T_n^{ND} f) = \mu(T_n^{AD} f) = \mu(f), \quad n = 1, 2, \ldots.$$

*Proof.* We prove only $\mu(T_n^{LD} f) = \mu(f)$, $n = 1, 2, \ldots$. The other two equalities are similar. Let $u^{(n)} = T_n^{LD} f$ and $u^{(n+1)} = T_{n+1}^{LD} f$. Then

$$(S + \triangle t W) u^{(n+1)} = S u^{(n)},$$

so

$$u^{(n+1)} = (S + \triangle t W)^{-1} S u^{(n)}.$$

By multiplying $S$ to the two sides of the above equation, we have

$$S u^{(n+1)} = (I + \triangle t W S^{-1})^{-1} S u^{(n)}.$$

Denote $v^{(n)} = S u^{(n)}$ and $A = (a_{ij}) = (I + \triangle t W S^{-1})^{-1}$; then

$$\begin{aligned} \mu(T_{n+1}^{LD} f) = \mu(u^{(n+1)}) &= \sum_i v_i^{(n+1)} = \sum_i \sum_j a_{ij} v_j^{(n)} \\ &= \sum_j \sum_i a_{ij} v_j^{(n)} = \sum_j v_j^{(n)} \sum_i a_{ij}. \end{aligned}$$

By the symmetry and vanishing row sums of $W$, it is easy to verify that $A$ is of unit column sums. This gives

$$\sum_i a_{ij} = 1 \quad \forall j.$$

Thus

$$\mu(T_{n+1}^{LD} f) = \sum_j v_j^{(n)} = \mu(u^{(n)}) = \mu(T_n^{LD} f) = \cdots = \mu(f). \qquad \blacksquare$$

**5.2.6. Information reduction, stability, and limit behavior.** In this subsection, we discuss the information reduction property of the discrete scale-spaces as well as their stability and limit behaviors. There are many ways to understand the information reduction (regularization) of scale-space evolution (or other similar procedures), such as low-pass filtering in frequency domain, entropy increasing, and energy minimizing, as well as diffusion. Our interpretation here is based on the eigenvalue and eigenvector analysis of matrices since we are in discrete settings.

First we give a lemma.

Lemma 5.7. *For the matrices $S, W, H(u^{(n)}), L(u^{(n)})$ in (5.1), (5.2), (5.3), the following hold:*

(1) *The eigenvalues of $S^{-1}W$ are $0 = \mu_1^{LD} < \mu_2^{LD} \le \cdots \le \mu_{\mathrm{V}}^{LD}$ with complete corresponding eigenvectors $\{(1,1,\ldots,1) = b_1^{LD}, b_2^{LD}, \ldots, b_{\mathrm{V}}^{LD}\}$. Furthermore,*

$$\mu_i^{LD} = \frac{\int_M |\nabla_M b_i^{LD}(p)|^2 dM}{(b_i^{LD})' S b_i^{LD}} \tag{5.8}$$

*for each $i$. Here $b_i^{LD}(p)$ is the piecewise linear interpolation of $b_i^{LD}$.*

(2) *The eigenvalues of $S^{-1}H(u^{(n)})$ are $0 = \mu_1^{ND} \le \mu_2^{ND} \le \cdots \le \mu_{\mathrm{V}}^{ND}$ with complete corresponding eigenvectors $\{(1,1,\ldots,1) = b_1^{ND}, b_2^{ND}, \ldots, b_{\mathrm{V}}^{ND}\}$. Furthermore,*

$$\mu_i^{ND} = \frac{\sum_\tau g(|\nabla_M u|_\tau^n|) \int_\tau |\nabla_M b_i^{ND}(p)|^2 d\tau}{(b_i^{ND})' S b_i^{ND}} \tag{5.9}$$

*for each $i$. And if the function $g(\cdot) > 0$, then $\mu_1^{ND} < \mu_2^{ND}$, and therefore $(1,1,\ldots,1)$ is the unique eigenvector of $\mu_1^{ND}$.*

(3) *The eigenvalues of $S^{-1}L(u^{(n)})$ are $0 = \mu_1^{AD} \le \mu_2^{AD} \le \cdots \le \mu_{\mathrm{V}}^{AD}$ with complete corresponding eigenvectors $\{(1,1,\ldots,1) = b_1^{AD}, b_2^{AD}, \ldots, b_{\mathrm{V}}^{AD}\}$. Furthermore,*

$$\mu_i^{AD} = \frac{\sum_\tau (g_1^n|_\tau \int_\tau (\nabla_M b_i^{AD}(p) \cdot e_1)^2 d\tau + g_2^n|_\tau \int_\tau (\nabla_M b_i^{AD}(p) \cdot e_2)^2 d\tau)}{(b_i^{AD})' S b_i^{AD}} \tag{5.10}$$

*for each $i$. And if the functions $g_1(\cdot) > 0$, $g_2(\cdot) > 0$, then $\mu_1^{AD} < \mu_2^{AD}$, and therefore $(1,1,\ldots,1)$ is the unique eigenvector of $\mu_1^{AD}$.*

*Proof.* We prove only (1). The proofs for (2) and (3) are similar by Theorem 5.1.

Since

$$S^{-1}W = \sqrt{S^{-1}}\sqrt{S^{-1}}W \sim (\sqrt{S^{-1}})^{-1}\sqrt{S^{-1}}\sqrt{S^{-1}}W\sqrt{S^{-1}} = \sqrt{S^{-1}}W\sqrt{S^{-1}},$$

by the symmetry of $W$, $S^{-1}W$ is similar to $\sqrt{S^{-1}}W\sqrt{S^{-1}}$, which is symmetric. This shows that all the eigenvalues of $S^{-1}W$ are real and the set of eigenvectors is complete.

Now assume $\mu$ is an eigenvalue of $S^{-1}W$ with corresponding eigenvector $b$. Then

$$S^{-1}Wb = \mu b \Rightarrow Wb = \mu Sb \Rightarrow b'Wb = \mu b'Sb \Rightarrow \mu = \frac{b'Wb}{b'Sb} = \frac{\int_M |\nabla_M b(p)|^2 dM}{b'Sb}$$

by Theorem 5.1. $\mu_1^{LD} = 0$ and $b_1^{LD} = (1,1,\ldots,1)$ follow immediately. ∎

With the same notation as in the above lemma, we have the following proposition.

Proposition 5.8. *In the linear, nonlinear, and anisotropic scale-spaces, the following hold:*

(1) *The eigenvalues of* $(I+\triangle tS^{-1}W)^{-1}$ *are* $1=\lambda_1^{LD}>\lambda_2^{LD}\geq\lambda_3^{LD}\geq\cdots\geq\lambda_{\mathrm{V}}^{LD}>0$ *with complete corresponding eigenvectors* $\{(1,1,\ldots,1)=b_1^{LD},b_2^{LD},\ldots,b_{\mathrm{V}}^{LD}\}$. *In addition,*

$$\lambda_i^{LD}=(1+\triangle t\mu_i^{LD})^{-1}. \tag{5.11}$$

(2) *The eigenvalues of* $(I+\triangle tS^{-1}H(u^{(n)}))^{-1}$ *are* $1=\lambda_1^{ND}\geq\lambda_2^{ND}\geq\lambda_3^{ND}\geq\cdots\geq\lambda_{\mathrm{V}}^{ND}>0$ *with complete corresponding eigenvectors* $\{(1,1,\ldots,1)=b_1^{ND},b_2^{ND},\ldots,b_{\mathrm{V}}^{ND}\}$, *and*

$$\lambda_i^{ND}=(1+\triangle t\mu_i^{ND})^{-1}. \tag{5.12}$$

*Furthermore, if the function* $g(\cdot)>0$, *then* $\lambda_1^{ND}>\lambda_2^{ND}$ *and* $(1,1,\ldots,1)$ *is the unique eigenvector of* $\lambda_1^{ND}$.

(3) *The eigenvalues of* $(I+\triangle tS^{-1}L(u^{(n)}))^{-1}$ *are* $1=\lambda_1^{AD}\geq\lambda_2^{AD}\geq\lambda_3^{AD}\geq\cdots\geq\lambda_{\mathrm{V}}^{AD}>0$ *with complete corresponding eigenvectors* $\{(1,1,\ldots,1)=b_1^{AD},b_2^{AD},\ldots,b_{\mathrm{V}}^{AD}\}$, *and*

$$\lambda_i^{AD}=(1+\triangle t\mu_i^{AD})^{-1}. \tag{5.13}$$

*Furthermore, if the functions* $g_1(\cdot)>0$, $g_2(\cdot)>0$, *then* $\lambda_1^{AD}>\lambda_2^{AD}$ *and* $(1,1,\ldots,1)$ *is the unique eigenvector of* $\lambda_1^{AD}$.

*Proof.* The assertion follows from the relationship between the eigenvalues and corresponding eigenvectors of $A$ and $(I+\triangle tA)^{-1}$ by Lemma 5.7. Here the matrix $A$ is any of $S^{-1}W$, $S^{-1}H(u^{(n)})$, $S^{-1}L(u^{(n)})$. ∎

Let us interpret the information reduction property of discrete scale-spaces, or the discrete filtering procedures, from Proposition 5.8. For a given initial image, it can be written into a linear combination of eigenvectors. As the scale $n$ increases, the components shrink along eigenvectors whose corresponding values are less than 1. Since all eigenvalues are less than or equal to 1, the only retained part is the component corresponding to the maximal eigenvalue 1. The maximal eigenvalue 1 corresponds to an eigenvector $(1,1,\ldots,1)$ which is the zero frequency of the signal. This zero frequency information will be preserved.

A careful investigation of the relationship between eigenvalues and their corresponding eigenvectors as shown in (5.8), (5.11), (5.9), (5.12), (5.10), and (5.13) gives us more deeper understanding. As for the linear scale-space, let us consider two components along eigenvectors $b_i^{LD}$ and $b_j^{LD}$ with eigenvalues $\lambda_i^{LD}>\lambda_j^{LD}$. Then the component along eigenvector $b_j^{LD}$ shrinks faster than that along $b_i^{LD}$. On the other hand, we have $\mu_j^{LD}>\mu_i^{LD}$ from (5.11); hence

$$\frac{\int_M|\nabla_M b_j^{LD}(p)|^2dM}{(b_j^{LD})'Sb_j^{LD}}>\frac{\int_M|\nabla_M b_i^{LD}(p)|^2dM}{(b_i^{LD})'Sb_i^{LD}}.$$

After normalization (and using the original notation), we have

$$\int_M|\nabla_M b_j^{LD}(p)|^2dM>\int_M|\nabla_M b_i^{LD}(p)|^2dM,$$

which shows that the $b_j^{LD}$ component is more irregular (or of higher frequency or larger Dirichlet energy) than the $b_i^{LD}$ component. Therefore, irregular components in the eigendecomposition of the image shrink faster than regular components.

Similar discussions for the discrete nonlinear scale-spaces point out some differences compared to the linear scale-spaces. Let us consider two components along eigenvectors $b_i^{ND}$ and $b_j^{ND}$ with $\lambda_i^{ND} > \lambda_j^{ND}$. On one hand, the component along eigenvector $b_j^{ND}$ shrinks faster than that along $b_i^{ND}$. On the other hand, we have $\mu_j^{ND} > \mu_i^{ND}$, which implies

$$\sum_{\tau} g(|\nabla_M u|_\tau^n|) \int_\tau |\nabla_M b_j^{ND}(p)|^2 d\tau > \sum_{\tau} g(|\nabla_M u|_\tau^n|) \int_\tau |\nabla_M b_i^{ND}(p)|^2 d\tau$$

after normalization. Note that the function $g$ is chosen to be decreasing with respect to the image intensity gradient. Unlike the linear scale-spaces, it is not necessary that components with larger Dirichlet energy shrink faster than those with lower Dirichlet energy. Besides the Dirichlet energy, the pixel spatial location contributing to the Dirichlet energy determines the shrink rate. Components with large Dirichlet energy contributed mainly by image edges and few oscillations (such as piecewise constant approximations of the image $u^{(n)}$) will shrink slowly. Meanwhile, those components with large Dirichlet energy contributed mainly by information of nonedges of the image such as spatially uniformly distributed small swing oscillations (noise, small scale textures) will shrink fast. Here we provide an explanation for the edge preserving of nonlinear filters via both global and local image structure analysis.

As for the anisotropic scale-spaces, the choice of $e_1, e_2$ and $g_1, g_2$ controls the information reduction effect of the discrete filter. Unlike the former two scale-spaces, here information can reduce anisotropically. From the expression of $\mu_i^{AD}$ in (5.10), one may choose appropriate $g_1, g_2$ to obtain the desired regularization effect. The analysis is similar to the above discussion but with one difference: the information reduction may be nonlinear as well as directional.

From Proposition 5.8 we can derive the following two results on the computational stability.

Corollary 5.9. *Assume $f$ is an initial image defined on a triangulated surface $M$. Then*

(1) $\|T_{n+1}^{LD} f\|_2 \le \|T_n^{LD} f\|_2$ *for any* $n = 0, 1, \ldots$;

(2) $\|T_{n+1}^{ND} f\|_2 \le \|T_n^{ND} f\|_2$ *for any* $n = 0, 1, \ldots$;

(3) $\|T_{n+1}^{AD} f\|_2 \le \|T_n^{AD} f\|_2$ *for any* $n = 0, 1, \ldots$.

*Proof.* The statement follows immediately from Proposition 5.8, since $\|Ax\|_2 \le \|A\|_2 \|x\|_2$ and $\|A\|_2 = \max_i |\lambda_i|$, where $\lambda_i$ is the eigenvalue of $A$. ∎

The above corollary gives the $L_2$ stability of linear, nonlinear, and anisotropic scale-spaces, while the following proposition shows that the gradient of the image in the scale-spaces remains bounded.

Proposition 5.10. *Given $f$ as an initial image, there exists a constant $C > 0$ such that $|\nabla_M T_n^{LD} f| \le C$, $|\nabla_M T_n^{ND} f| \le C$, and $|\nabla_M T_n^{AD} f| \le C$ for $n = 1, 2, \ldots$.*

*Proof.* We consider only the linear scale-space. The arguments for the other two are similar by Corollary 5.9. We first recall

$$\int_M |\nabla_M (T_n^{LD} f)(p)|^2 dM = \sum_{\tau=[v_i,v_j,v_k]} s_\tau |\nabla_M (T_n^{LD} f)|_\tau^2 = (T_n^{LD} f)' W (T_n^{LD} f)$$

from Theorem 5.1, where $s_\tau$ is the area of triangle $\tau$. Since $W$ is a symmetric matrix, $W$ is orthogonally similar to a diagonal matrix. Assume $\mu_1, \mu_2, \ldots, \mu_V$ are the eigenvalues of

$W$ and $b_1, b_2, \ldots, b_{\mathrm{V}}$ are their corresponding eigenvectors. $\{b_1, b_2, \ldots, b_{\mathrm{V}}\}$ form an orthogonal basis. Therefore, $T_n^{LD} f$ can be decomposed as

$$T_n^{LD} f = \sum_{1 \le i \le \mathrm{V}} \alpha_i^{(n)} b_i.$$

Thus we have

$$\begin{aligned} &\int_M |\nabla_M (T_n^{LD} f)(p)|^2 dM \\ &= (T_n^{LD} f)' W (T_n^{LD} f) = \sum_{1 \le i \le \mathrm{V}} \mu_i (\alpha_i^{(n)})^2 \le \max_{1 \le i \le \mathrm{V}} \mu_i \sum_{1 \le i \le \mathrm{V}} (\alpha_i^{(n)})^2 \\ &= \max_{1 \le i \le \mathrm{V}} \mu_i \|T_n^{LD} f\|_2^2 \le \max_{1 \le i \le \mathrm{V}} \mu_i \|T_{n-1}^{LD} f\|_2^2 \le \cdots \le \max_{1 \le i \le \mathrm{V}} \mu_i \|f\|_2^2 \end{aligned}$$

for any $n$. Therefore,

$$|\nabla_M (T_n^{LD} f)|^2 \le \frac{\max_{1 \le i \le \mathrm{V}} \mu_i \|f\|_2^2}{\min_\tau s_\tau} \doteq C_1.$$

Choose $C = \sqrt{C_1}$. ■

Note that Corollary 5.9 and Proposition 5.10 indicate the stability of our method, in spite of the possible ill-posedness of the PDE with special diffusivities such as Perona–Malik models.

The information reduction effect is particularly evident in the linear scale-space and in the nonlinear and anisotropic scale-spaces when $g(\cdot) > 0$, $g_1(\cdot) > 0$, $g_2(\cdot) > 0$. In these cases, the retained component is along direction $(1, 1, \ldots, 1)$, which is the unique eigenvector corresponding to the eigenvalue 1. It serves as a constant function and results in a limit behavior of the discrete scale-spaces.

Proposition 5.11. *For an initial image $f$, let $\mu(f)$ be the total grey defined in (5.7) and $s_i$ be the area of the control cell of $v_i$. Then*

(1) $\lim_{n\to\infty} T_n^{LD} f = \frac{\mu(f)}{\sum_{i=0,1,\ldots,\mathrm{V}-1} s_i}(1, 1, \ldots, 1)$;

(2) *if $g(\cdot) > 0$,* $\lim_{n\to\infty} T_n^{ND} f = \frac{\mu(f)}{\sum_{i=0,1,\ldots,\mathrm{V}-1} s_i}(1, 1, \ldots, 1)$;

(3) *if $g_1(\cdot) > 0$, $g_2(\cdot) > 0$,* $\lim_{n\to\infty} T_n^{AD} f = \frac{\mu(f)}{\sum_{i=0,1,\ldots,\mathrm{V}-1} s_i}(1, 1, \ldots, 1)$.

*Proof.* (1) By Proposition 5.6, one need only prove that the limit of $T_n^{LD} f$ is a constant function. From Proposition 5.8, the components of $f$ corresponding to eigenvectors whose eigenvalues are less than 1 will shrink and vanish eventually. The only retained part is the component corresponding to eigenvector $(1, 1, \ldots, 1)$, which is unique to the eigenvalue 1. This demonstrates that the limit is a constant function.

(2) Although $g(\cdot) > 0$, we cannot obtain the result using the same argumentation as in (1) by Proposition 5.8. In the nonlinear scale-space, the eigenvalues and eigenvectors are variational along with the iteration since $H(u^{(n)})$ depends on $u^{(n)}$. We reformulate the scale-space evolution (5.2) to be

$$(\sqrt{S} + \triangle t \sqrt{S^{-1}} H(u^{(n)})) u^{(n+1)} = \sqrt{S} u^{(n)},$$

from which we further have

$$\sqrt{S} u^{(n+1)} + \triangle t \sqrt{S^{-1}} H(u^{(n)}) \sqrt{S^{-1}} \sqrt{S} u^{(n+1)} = \sqrt{S} u^{(n)}. \tag{5.14}$$

Let $y^{(n)} = \sqrt{S}u^{(n)}$. The above equation is actually

$$(I + \triangle t\sqrt{S^{-1}}H(\sqrt{S^{-1}}y^{(n)})\sqrt{S^{-1}})y^{(n+1)} = y^{(n)}. \tag{5.15}$$

In the following we find out the limit of $y^{(n)}$, from which the limit of $u^{(n)}$ can be deduced.

We first show the structure of the eigenvalues and eigenvectors of $\sqrt{S^{-1}}H(u^{(n)})\sqrt{S^{-1}}$ (or $\sqrt{S^{-1}}H(\sqrt{S^{-1}}y^{(n)})\sqrt{S^{-1}}$). By the symmetry, $\sqrt{S^{-1}}H(\sqrt{S^{-1}}y^{(n)})\sqrt{S^{-1}}$ is orthogonally similar to a diagonal matrix. We then assume the eigenvalues and corresponding eigenvectors are $\lambda_1^{(n)} \le \lambda_2^{(n)} \le \cdots \le \lambda_{\mathrm{V}}^{(n)}$ and $b_1^{(n)}, b_2^{(n)}, \ldots, b_{\mathrm{V}}^{(n)}$. Since $\sqrt{S^{-1}}H(\sqrt{S^{-1}}y^{(n)})\sqrt{S^{-1}} \sim S^{-1}H(\sqrt{S^{-1}}y^{(n)})$, we know $0 = \lambda_1 = \lambda_1^{(n)} < \lambda_2^{(n)} \le \cdots \le \lambda_{\mathrm{V}}^{(n)}$ and $b_1^{(n)} = \sqrt{S}(1, 1, \ldots, 1)' = b_1$, by Lemma 5.7. Note that $b_1^{(n)}$ and $\lambda_1^{(n)}$ are independent of $n$ and are sometimes written as $b_1$ and $\lambda_1$.

Moreover, we further demonstrate that the second smallest eigenvalue $\lambda_2^{(n)} > C$ for some constant $C$ independent of $n$. Our strategy is to compare the eigenvalues of $\sqrt{S^{-1}}H(u^{(n)})\sqrt{S^{-1}}$ and $\sqrt{S^{-1}}W\sqrt{S^{-1}}$ via their Rayleigh quotients [17], since the eigenvalues of $\sqrt{S^{-1}}W\sqrt{S^{-1}} \sim S^{-1}W$ are independent of iterations and greater than or equal to zero by Lemma 5.7. In addition, $\sqrt{S^{-1}}W\sqrt{S^{-1}}$ has the unique eigenvector $b_1$ corresponding to the smallest eigenvalue $\lambda_1$, just like $\sqrt{S^{-1}}H(u^{(n)})\sqrt{S^{-1}}$. Consider the Rayleigh quotients

$$R_{\sqrt{S^{-1}}H(u^{(n)})\sqrt{S^{-1}}}(x) = \frac{x'\sqrt{S^{-1}}H(u^{(n)})\sqrt{S^{-1}}x}{x'x}$$

and

$$R_{\sqrt{S^{-1}}W\sqrt{S^{-1}}}(x) = \frac{x'\sqrt{S^{-1}}W\sqrt{S^{-1}}x}{x'x},$$

where $x$ is a vector. According to equation (4.2.7) on page 178 of [17], we have

$$\lambda_2(\sqrt{S^{-1}}H(u^{(n)})\sqrt{S^{-1}}) = \min_{x\neq 0, x\perp b_1} \frac{x'\sqrt{S^{-1}}H(u^{(n)})\sqrt{S^{-1}}x}{x'x}$$

and

$$\lambda_2(\sqrt{S^{-1}}W\sqrt{S^{-1}}) = \min_{x\neq 0, x\perp b_1} \frac{x'\sqrt{S^{-1}}W\sqrt{S^{-1}}x}{x'x},$$

where $\lambda_2(A)$ stands for the second smallest eigenvalue of $A$. Note that the second smallest eigenvalues of both $\sqrt{S^{-1}}H(u^{(n)})\sqrt{S^{-1}}$ and $\sqrt{S^{-1}}W\sqrt{S^{-1}}$ are the minimal values of their Rayleigh quotients restricted in the same subset, respectively.

On the other hand, we know the gradient of the image in the scale-space is bounded from Proposition 5.10. Denoting the bound as $C_1$, that is, $|\nabla_M u^{(n)}| \le C_1$ for any $n$, we have

$$g(C_1)x'\sqrt{S^{-1}}W\sqrt{S^{-1}}x \le x'\sqrt{S^{-1}}H(u^{(n)})\sqrt{S^{-1}}x \le g(0)x'\sqrt{S^{-1}}W\sqrt{S^{-1}}x.$$

This shows that

$$\lambda_2^{(n)} = \lambda_2(\sqrt{S^{-1}}H(u^{(n)})\sqrt{S^{-1}}) \ge g(C_1)\lambda_2(\sqrt{S^{-1}}W\sqrt{S^{-1}}) \doteq C, \tag{5.16}$$

where $C > 0$, since $\lambda_2(\sqrt{S^{-1}}W\sqrt{S^{-1}}) > 0$ and $g(\cdot) > 0$.

We then come back to the scale-space evolution. $y^{(n)}$ can be decomposed as

$$y^{(n)} = \sum_{1\le i\le \mathrm{V}} \alpha_i^{(n)} b_i^{(n)}.$$

By (5.15), we obtain

$$\sum_{1\le i\le \mathrm{V}} \alpha_i^{(n+1)} b_i^{(n+1)} = y^{(n+1)} = \sum_{1\le i\le \mathrm{V}} (1+\triangle t\lambda_i^{(n)})^{-1}\alpha_i^{(n)} b_i^{(n)},$$

where $\{b_1^{(n+1)}, b_2^{(n+1)}, \ldots, b_{\mathrm{V}}^{(n+1)}\}$ are the eigenvectors of $\sqrt{S^{-1}}H(u^{(n+1)})\sqrt{S^{-1}}$ for the scale-space evolution from $y^{(n+1)}$ to $y^{(n+2)}$. Hence we deduce $\alpha_1^{(n+1)} = \alpha_1^{(n)}$ since $b_1^{(n+1)} = b_1^{(n)} = b_1$ and $b_1$ is orthogonal to other vectors. We also have

$$\|y^{(n+1)}\|^2 = (\alpha_1^{(n)})^2 + \sum_{2\le i\le \mathrm{V}} (1+\triangle t\lambda_i^{(n)})^{-2}(\alpha_i^{(n)})^2,$$

yielding

$$\begin{aligned} 0 \le \|y^{(n+1)}\|^2 - (\alpha_1^{(n+1)})^2 &\le (1+\triangle tC)^{-2}(\|y^{(n)}\|^2 - (\alpha_1^{(n)})^2) \\ &\le (1+\triangle tC)^{-4}(\|y^{(n-1)}\|^2 - (\alpha_1^{(n-1)})^2) \\ &\le \cdots \\ &\le (1+\triangle tC)^{-2(n+1)}(\|f\|^2). \end{aligned}$$

Sending $n\to\infty$ and taking into account that $\alpha_1$ corresponds to the eigenvector $b_1$, we see the limit of $y^{(n)}$ is along $b_1$. Therefore the limit of $u^{(n)}$ is along $(1,1,\ldots,1)$, from which the assertion follows.

(3) The statement can be verified in a similar way with the above procedure by noticing

$$\begin{aligned} v'L(u^{(n)})v &= \sum_{\tau}\left(g_1^n|_\tau \int_\tau (\nabla_M v(p)\cdot e_1)^2 d\tau + g_2^n|_\tau \int_\tau (\nabla_M v(p)\cdot e_2)^2 d\tau\right) \\ &\ge \sum_{\tau} \min(g_1^n|_\tau, g_2^n|_\tau)\left(\int_\tau (\nabla_M v(p)\cdot e_1)^2 d\tau + \int_\tau (\nabla_M v(p)\cdot e_2)^2 d\tau\right) \\ &= \sum_{\tau} \min(g_1^n|_\tau, g_2^n|_\tau)\int_\tau |\nabla_M v(p)|^2 d\tau \end{aligned}$$

as calculated in Theorem 5.1. ■

The above proposition predicts a constant limit behavior of these scale-spaces or the corresponding filtering procedures when the scale $n\to\infty$. It gives users some suggestions. First, some fidelity terms have to be added into the filtering models to preserve some particular and valuable features of the original images just as is done in most of our applications [61]. Second, to avoid the constant limit direction, one can carefully design the functions $g_1, g_2$ and the piecewise vector fields $e_1, e_2$. For example, one can set $g_1$ or $g_2$ to be zero or very small to keep the features along $e_1$ or $e_2$. This explains the configurations of diffusion models when applied to directional texture generating [61] and anisotropic image anti-aliasing and denoising (see the examples in section 6).

**5.2.7. Maximum-minimum principle.** In this subsection, we will prove the maximum-minimum principle for the discrete linear and nonlinear scale-spaces if there are no obtuse triangles in the triangulated surface $M$.

Proposition 5.12. *Suppose that there are no obtuse triangles in the triangulated surface $M$. Let $f$ be an initial image and*

$$m(f) := \min_{j=0,1,\ldots,\mathrm{V}-1} f_j,$$
$$M(f) := \max_{j=0,1,\ldots,\mathrm{V}-1} f_j;$$

*then*

(1) $m(f) \le (T_n^{LD} f)_i \le M(f)$ *for* $i = 0, 1, \ldots, \mathrm{V}-1$, $n = 1, 2, \ldots$;
(2) $m(f) \le (T_n^{ND} f)_i \le M(f)$ *for* $i = 0, 1, \ldots, \mathrm{V}-1$, $n = 1, 2, \ldots$.

*Proof.* We prove only (1) ((2) can be proved similarly). Let $u^{(n)} = T_n^{LD} f$ and $u^{(n+1)} = T_{n+1}^{LD} f$; then

$$(S + \triangle t W) u^{(n+1)} = S u^{(n)},$$

so

$$\begin{aligned} u^{(n+1)} &= (S + \triangle t W)^{-1} S u^{(n)} \\ &= (I + \triangle t S^{-1} W)^{-1} u^{(n)} := A u^{(n)}, \end{aligned}$$

where $A = (a_{ij})_{\mathrm{V}\times\mathrm{V}}$. Since $M$ does not have obtuse triangles and $W$ is positive semidefinite, it is obvious that $I + \triangle t S^{-1} W$ is an M-matrix [46]. Therefore elements of $A$ are all nonnegative. On the other hand, one can easily verify that the sum of each row of $I + \triangle t S^{-1} W$ is unit, and hence of $A$. Therefore,

$$u_i^{(n+1)} = \sum_j a_{ij} u_j^{(n)} \le \sum_j a_{ij} \max_j u_j^{(n)} \le \max_j u_j^{(n)}$$

and

$$u_i^{(n+1)} = \sum_j a_{ij} u_j^{(n)} \ge \sum_j a_{ij} \min_j u_j^{(n)} \ge \min_j u_j^{(n)}$$

hold for all $i$ and $n$. The assertion follows this immediately. ∎

It should be pointed out that the maximum-minimum principle may not hold for the discrete anisotropic scale-spaces, since they depend on the choice of $e_1, e_2$ and $g_1, g_2$.

**5.2.8. Remark.** In the analysis so far, we have assumed that in the anisotropic diffusion model the vector fields $e_1, e_2$ are kept fixed. We want to emphasize that the analysis is still true if $e_1, e_2$ depend on time $t$ and the solution $u$, i.e., $e_1 = e_1(x, t, u)$, $e_2 = e_2(x, t, u)$. However, the computation is much more complicated since the coefficients $\{c_{ii,\tau}^1, c_{ij,\tau}^1, c_{ik,\tau}^1, c_{ii,\tau}^2, c_{ij,\tau}^2, c_{ik,\tau}^2, c_{ji,\tau}^1, c_{jj,\tau}^1, c_{jk,\tau}^1, c_{ji,\tau}^2, c_{jj,\tau}^2, c_{jk,\tau}^2, c_{ki,\tau}^1, c_{kj,\tau}^1, c_{kk,\tau}^1, c_{ki,\tau}^2, c_{kj,\tau}^2, c_{kk,\tau}^2\}$ should be updated in each iteration.

**6. Examples and discussion.** In this section, several examples are provided to illustrate the differences for the different discrete filtering procedures on triangulated surfaces. In particular, we make comparisons between linearity and nonlinearity, as well as isotropic and anisotropic procedures.

In the first and second examples, we compute discrete linear and nonlinear scale-spaces of the initial image of Lena defined on an open mesh surface (a discrete manifold with a boundary where boundary conditions of diffusion equations should be considered) and a color image painted on a bunny surface (which is closed and complex and has genus zero) as illustrated in Figures 4, 5, 6, 7, 8, and 9, respectively. For the nonlinear scale-spaces, we choose three diffusivities for the function $g(s)$ from Table 1. They are $\frac{1}{\sqrt{s^2+\beta}}$, $\frac{1}{1+(\frac{s}{K})^2}$, and $\frac{1}{s^2+\beta}$. In each figure, the images from top left to bottom right represent increasing scales. As one can see, topologies of images in the scale-spaces get simpler when scales get larger regardless of linearity and nonlinearity. This information reduction property is basic for the scale-spaces of planar images and is preserved for images over mesh surfaces. In addition, other properties such as the constant limit behavior and the maximum-minimum principle can also be observed. However, there are still many differences between the linear and nonlinear filtering or their corresponding discrete scale-spaces. They both simplify topologies of images but behave in different ways. In the linear scale-space, the initial image is smoothed isotropically, while in the nonlinear scale-space the initial image is smoothed nonlinearly and locally. Hence different effects appear. In images of linear scale-spaces, different objects are syncretized, and they become more and more indistinguishable. In images of nonlinear scale-spaces, texture-like finer details disappear gradually and piecewise constant functions form. If the scale gets even larger (see our second example in which there are no details at all in the initial image), the piecewise constant functions will become more simplified in such a way that patches with similar grey levels merge with each other, and patches with large sizes swallow nearby small patches. This is to be expected since the chosen $g$ function is decreasing with respect to the image intensity gradient, and the total (or weighted average) grey level is preserved as proved in Proposition 5.6. One even can observe clearly the differences between the nonlinear filterings with different diffusivities from Figures 5, 6, and 7. According to Table 1, the regularized TV flow is a pure diffusion procedure, whereas the Perona–Malik and balanced forward-backward (BFB) diffusivities are smoothing/enhancing models. In other words, Perona–Malik and BFB models sharpen image edges when smoothing homogeneous regions of the image. The BFB model even generates false image edges as shown in Figure 7. In spite of this, the image sequence in the scale-spaces will tend to a constant function. The speed of this procedure depends on the diffusivity $g$ or, more precisely, $\frac{g(s)}{g(s)+sg'(s)}$, the ratio of the diffusion coefficients along the tangential and normal directions of the level sets of the image intensity. From this ratio one can figure out why the image sequence in Figure 6 approaches the constant limit much faster than that in Figure 7. Actually, this fact demonstrates that in image restoration problems the BFB model sometimes behaves better than other models, especially for images containing multiscale edges.

Examples about anisotropic discrete filtering procedures with different constant diffusion rates are provided in Figures 10, 11, 12, 13, and 14. In the sphere example, we chose $e_1$ to be the longitude and $e_2$ the latitude of the sphere. We calculated three discrete anisotropic scale-spaces with low, middle, and high anisotropies, respectively, as shown in Figures 10, 11,

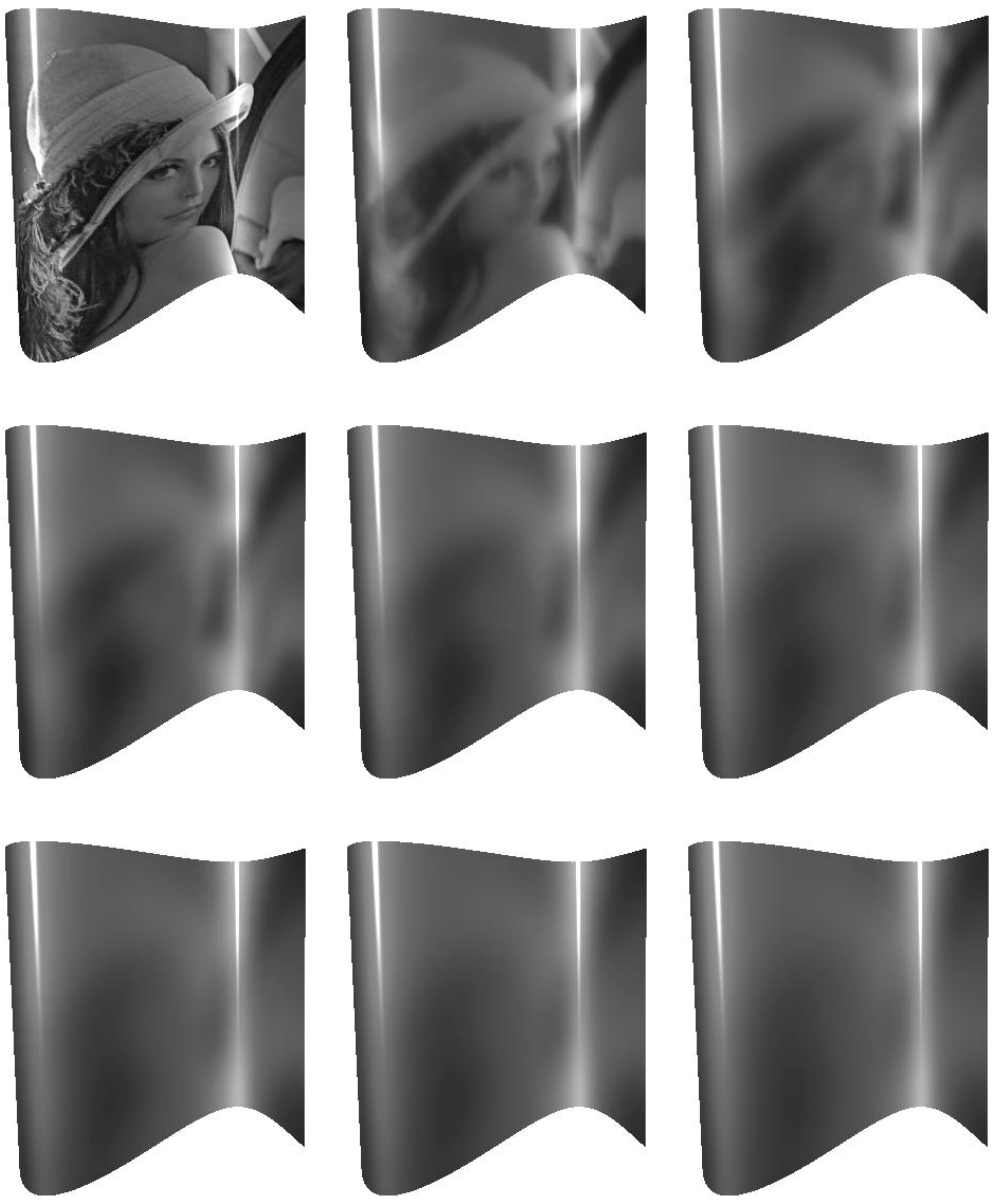

**Figure 4.** *Discrete linear scale-space of Lena on an open surface. From top left to bottom right, the discrete scales are* 0, 1, 3, 5, 7, 9, 11, 13, 16, *respectively.*

and 12. As demonstrated in our analysis, information of the initial image is reduced when the scale increases. And if $g_1 > 0$, $g_2 > 0$, the initial image will tend to a constant limit. If one wishes to keep image features along some direction, one just sets the diffusion rate of that direction to be zero. Figure 12, in which $g_1 = 0$, is such an example. This results in no filtering along the $e_1$ direction, the longitude of the sphere. Along the latitude of the

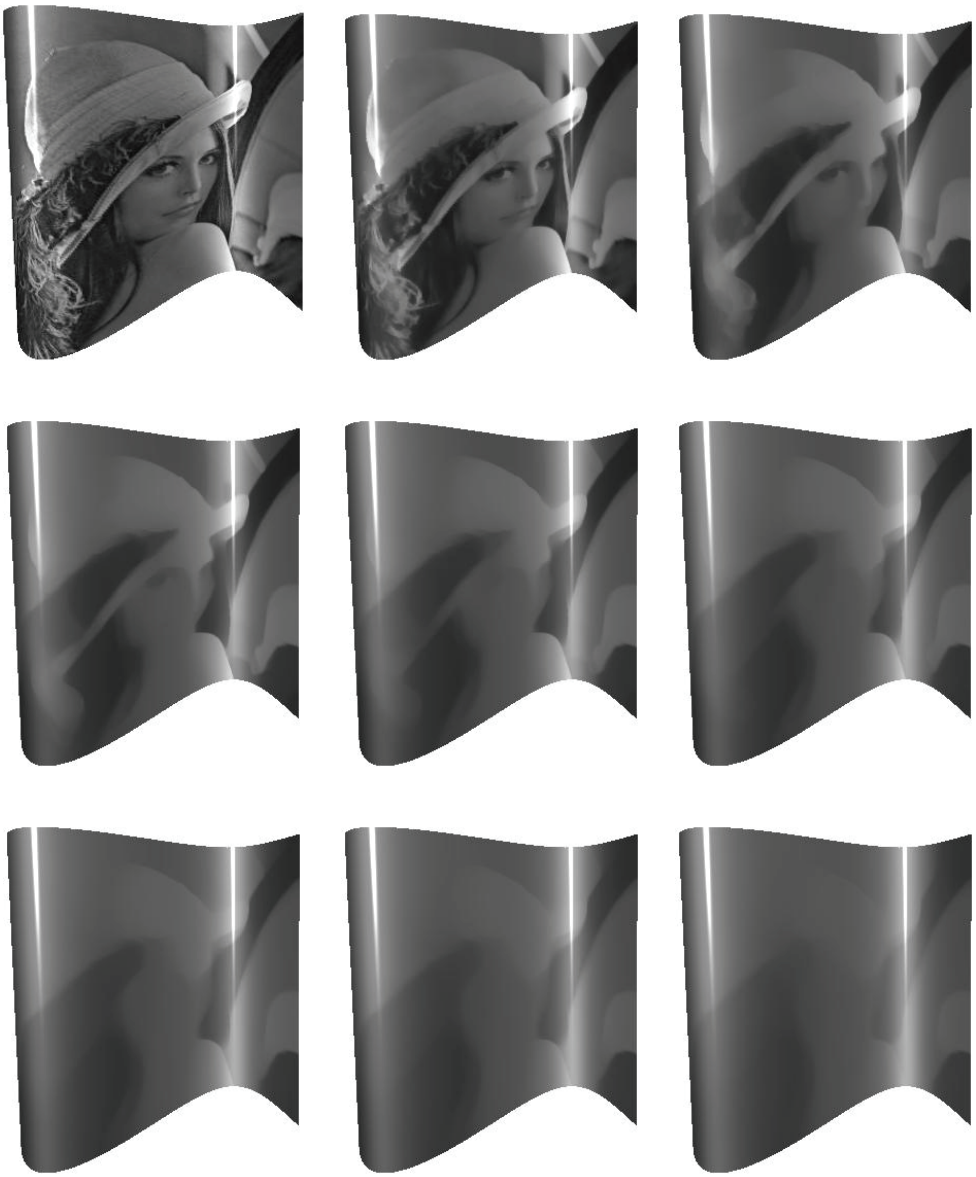

**Figure 5.** *Discrete nonlinear scale-space* ($g(s) = \frac{1}{\sqrt{s^2+\beta}}$ *with* $\beta = 10^{-10}$*, regularized total variation flow) of Lena on an open surface. From top left to bottom right, the discrete scales are* 0, 1, 3, 5, 7, 9, 11, 13, 16, *respectively.*

sphere $e_2$, the choice of $g_2 = 1$ smoothes out the zigzag edge and gives an anti-aliasing effect. These observations can also be found in the Utah teapot example (see Figure 13). A careless colorization yields a zigzag edge between the white cover and the grey body; see the zoom-in in Figure 13. We computed three filtering procedures for the zigzag removal as shown in Figure 14.

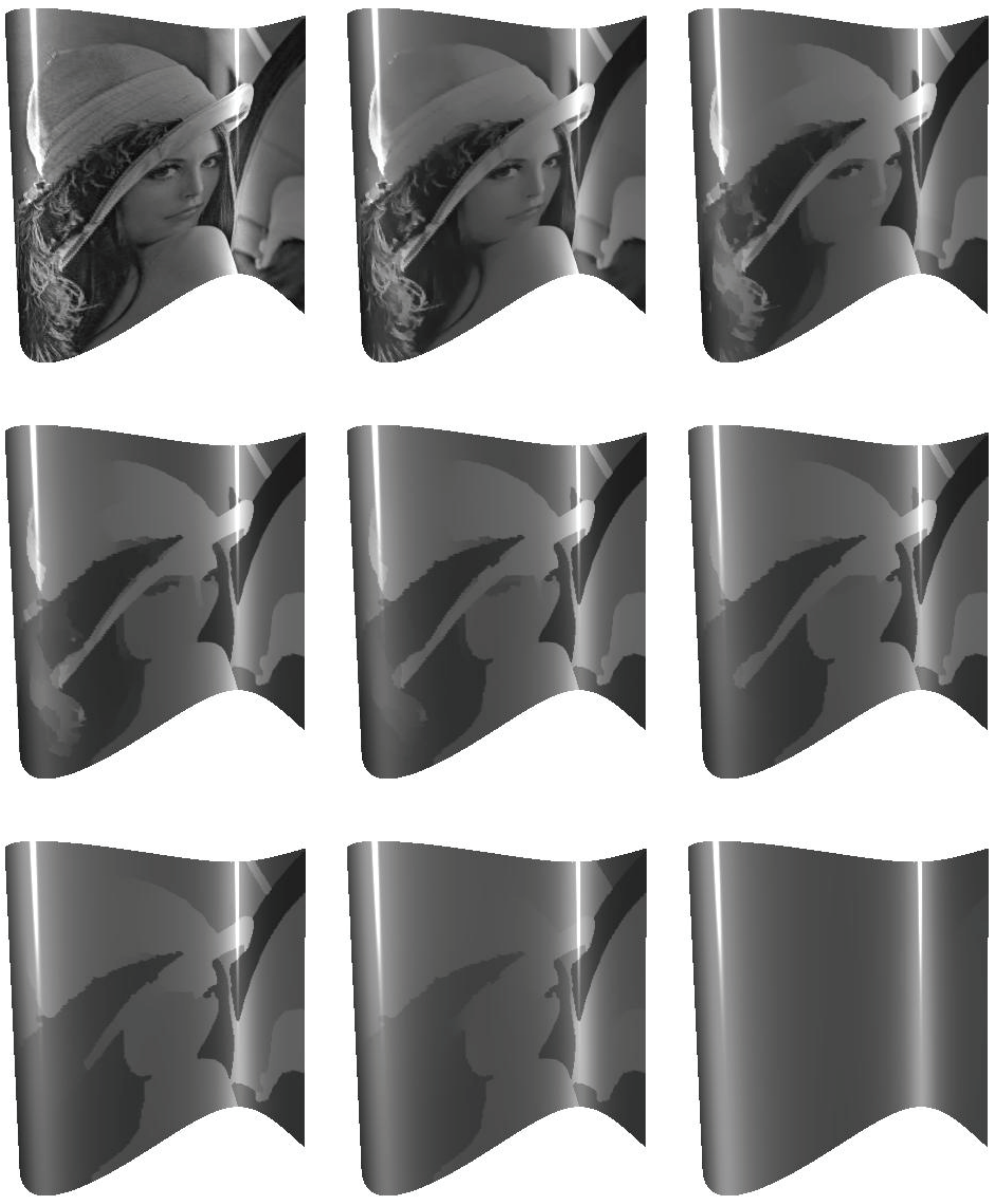

**Figure 6.** *Discrete nonlinear scale-space* ($g(s) = \frac{1}{1+(\frac{s}{K})^2}$ *with* $K = 1$, *one of the Perona–Malik diffusivities) of Lena on an open surface. From top left to bottom right, the discrete scales are* 0, 1, 3, 5, 7, 9, 13, 20, 50, *respectively.*

The last example shows the anisotropic discrete filtering applied to simultaneously anti-aliasing and denoising; see Figure 15. The first row is the noisy image with zigzag aliasing along the latitude direction. Again we choose the longitude to be $e_1$ and the latitude to be $e_2$. Three anisotropic scale-spaces with different $g_1, g_2$ as stated in the figure are computed

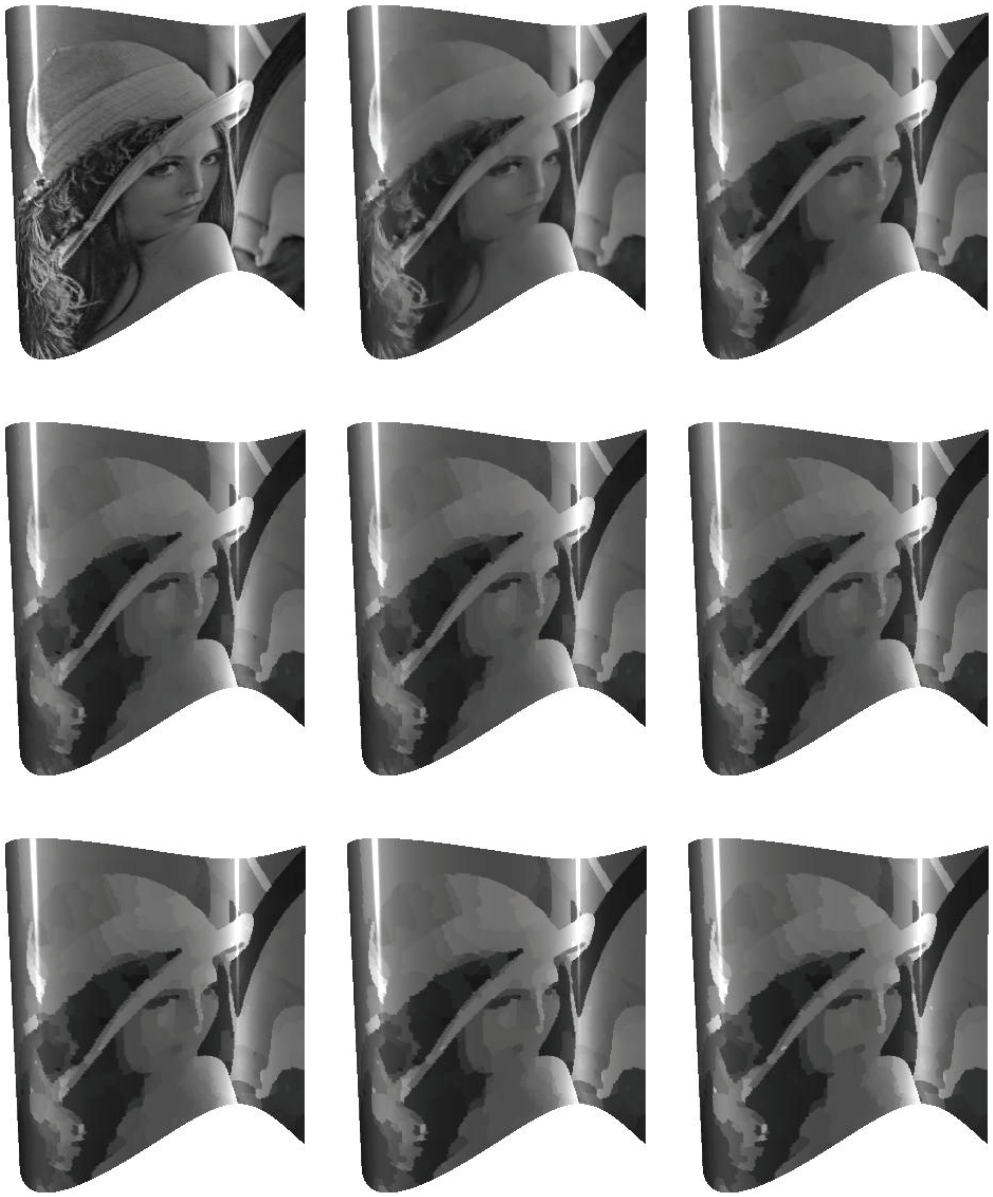

**Figure 7.** *Discrete nonlinear scale-space* ($g(s) = \frac{1}{s^2+\beta}$ *with* $\beta = 10^{-5}$*, a regularized BFB diffusivity) of Lena on an open surface. From top left to bottom right, the discrete scales are* 0, 1, 3, 20, 50, 100, 500, 1000, 2000*, respectively.*

and compared. As one can see, the results are quite different between different scale-spaces. In the anisotropic filtering for pure anti-aliasing (second row), the zigzag disappears very quickly, whereas the noise tends to be directional. In the pure denoising procedure (third row), the image noise is removed quite quickly, but the zigzag aliasing changes slowly (for the

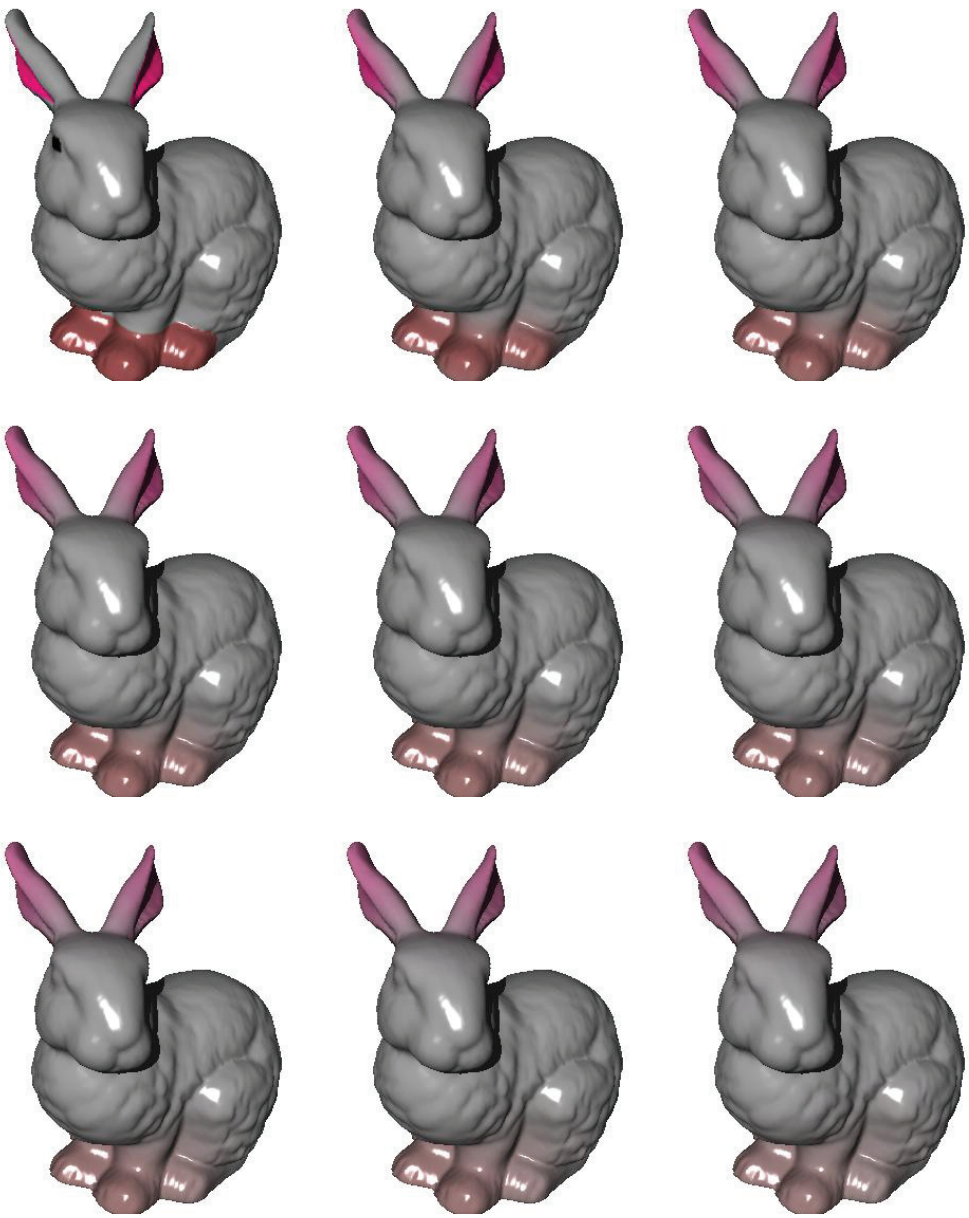

**Figure 8.** *Discrete linear scale-space of an image on the bunny. From top left to bottom right, the discrete scales are* 0, 3, 6, 9, 12, 15, 18, 21, 30, *respectively.*

edge-preserving diffusivity). By combining these two procedures, we can get the much better result as shown in the fourth row, in which the noise and zigzag aliasing vanish simultaneously. Actually, this is philosophically reasonable since we know the information of both the noise and the aliasing in this example.

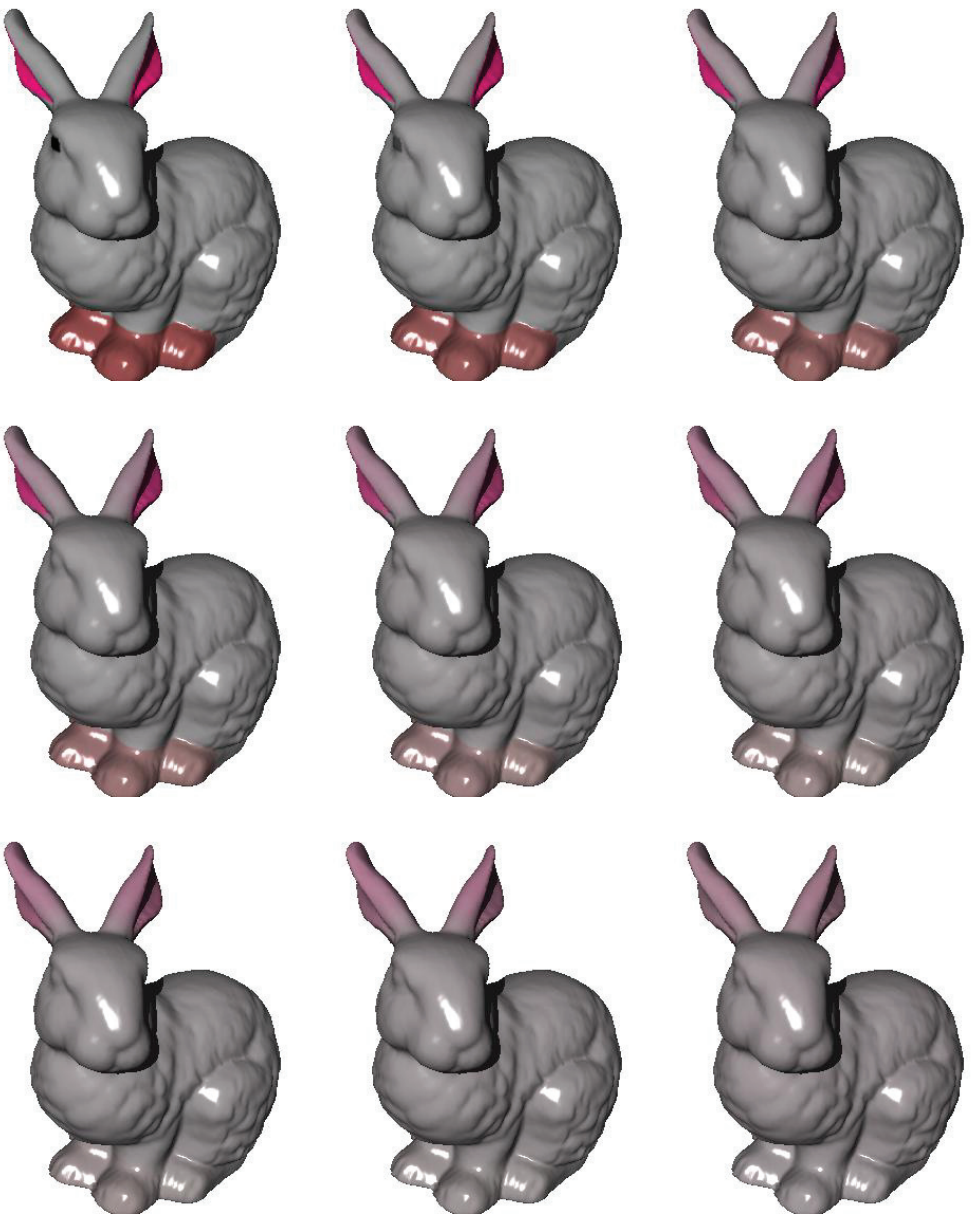

**Figure 9.** *Discrete nonlinear scale-space* ($g(s) = \frac{1}{\sqrt{s^2+\beta}}$ *with* $\beta = 10^{-10}$*, regularized TV flow) of an image on the bunny. From top left to bottom right, the discrete scales are* 0, 3, 6, 9, 12, 15, 18, 21, 30*, respectively. Note the color change on the body and feet of the bunny, when compared with the linear scale-space in Figure* 8.

**7. Conclusions and future work.** In this paper, we provide scale-space analysis for discrete linear, nonlinear, and anisotropic filtering procedures over triangulated surfaces. We start by presenting diffusion equations on smooth manifolds. Using appropriately defined differential operators on triangulated surfaces, we then derive the discrete filtering schemes.

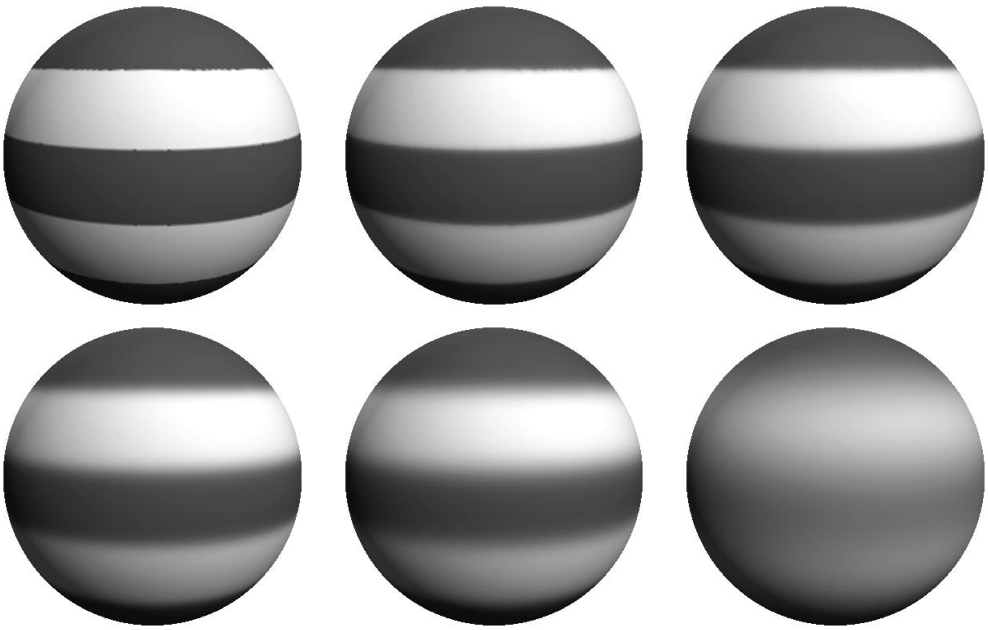

**Figure 10.** *Discrete anisotropic scale-space of an image on a unit sphere.* $e_1$*: the longitude.* $e_2$*: the latitude.* $g_1 = g_2 = 1$*. From top left to bottom right, the discrete scales are* 0, 1, 2, 5, 10, 100*, respectively.*

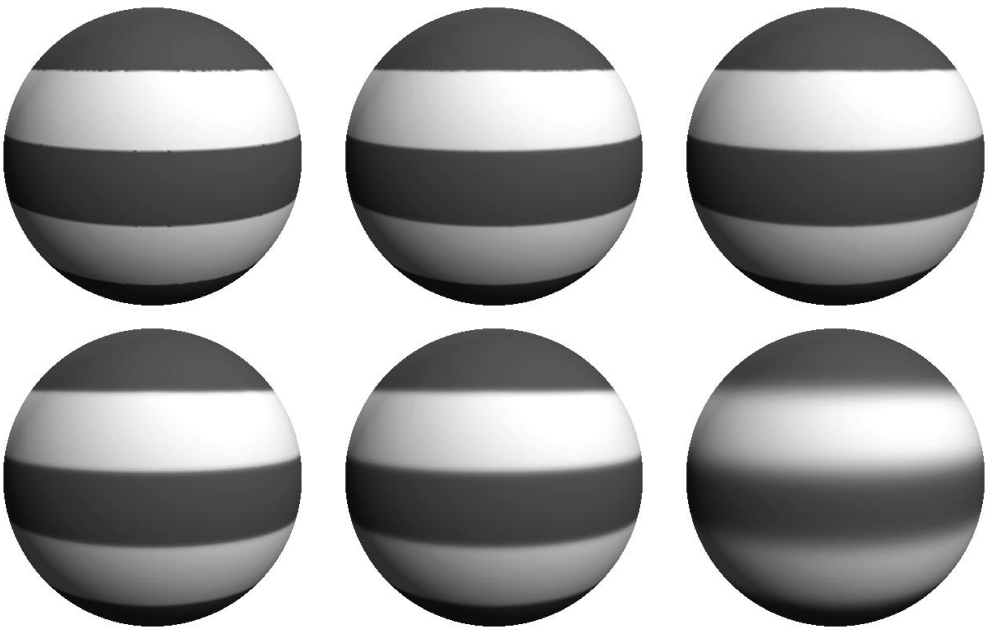

**Figure 11.** *Discrete anisotropic scale-space of an image on a unit sphere.* $e_1$*: the longitude.* $e_2$*: the latitude.* $g_1 = 0.1$*,* $g_2 = 1$*. From top left to bottom right, the discrete scales are* 0, 1, 2, 5, 10, 100*, respectively.*

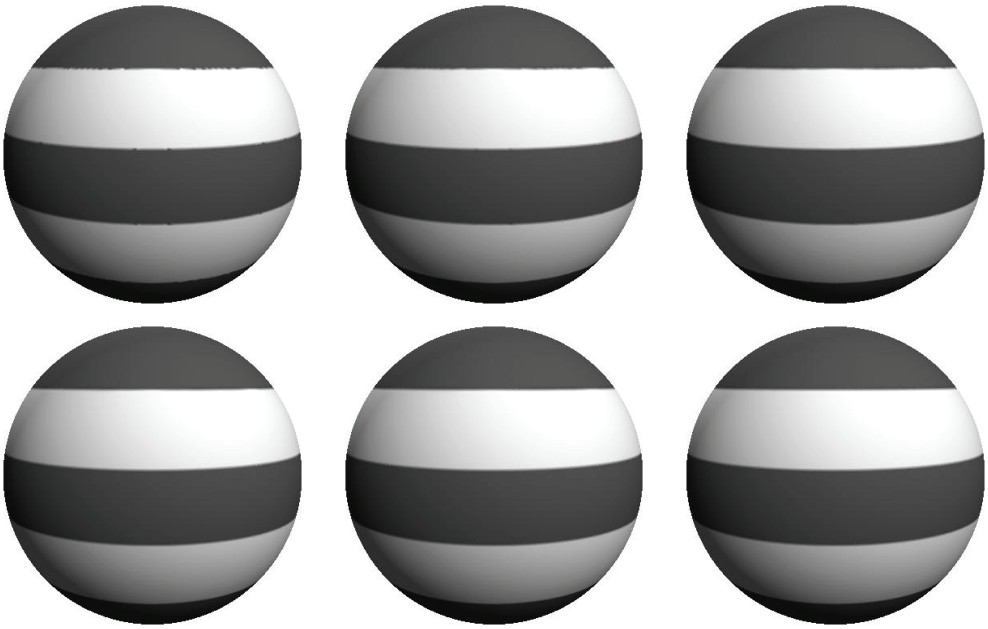

**Figure 12.** *Discrete anisotropic scale-space of an image on a unit sphere.* $e_1$*: the longitude.* $e_2$*: the latitude.* $g_1 = 0$, $g_2 = 1$. *From top left to bottom right, the discrete scales are* 0, 1, 2, 5, 10, 100, *respectively.*

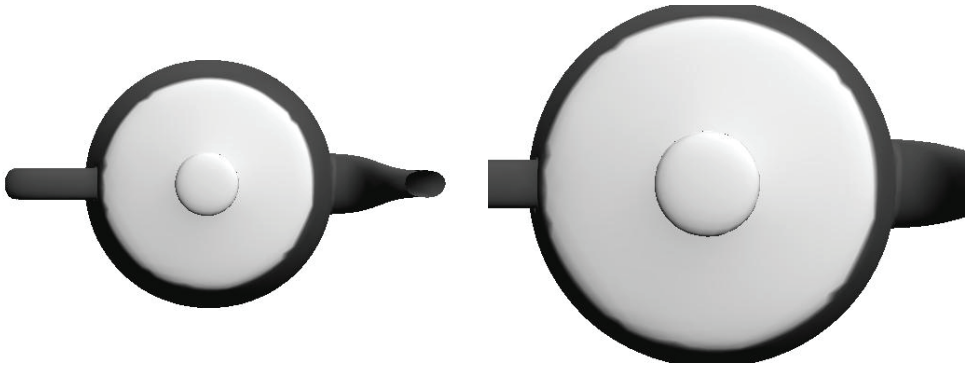

**Figure 13.** *An image on the Utah teapot model and its zoom-in.*

These filtering schemes are analyzed with discrete scale-space concepts. Several properties are discussed and proved, such as existence and uniqueness, continuous dependence on initial value, the discrete semigroup property, information reduction, and limit behavior, as well as computational stability. In particular, we use eigenvalue and eigenvector analysis of matrices to interpret the information reduction property and the limit behavior. Linear and nonlinear filtering, as well as isotropic and anisotropic filtering, are compared by considering the eigenvalues and eigenvectors of the discrete scale-space matrices. Experiments support our analysis and interpretation.

Some problems are left open. The first is to extend the three types of scale-spaces to

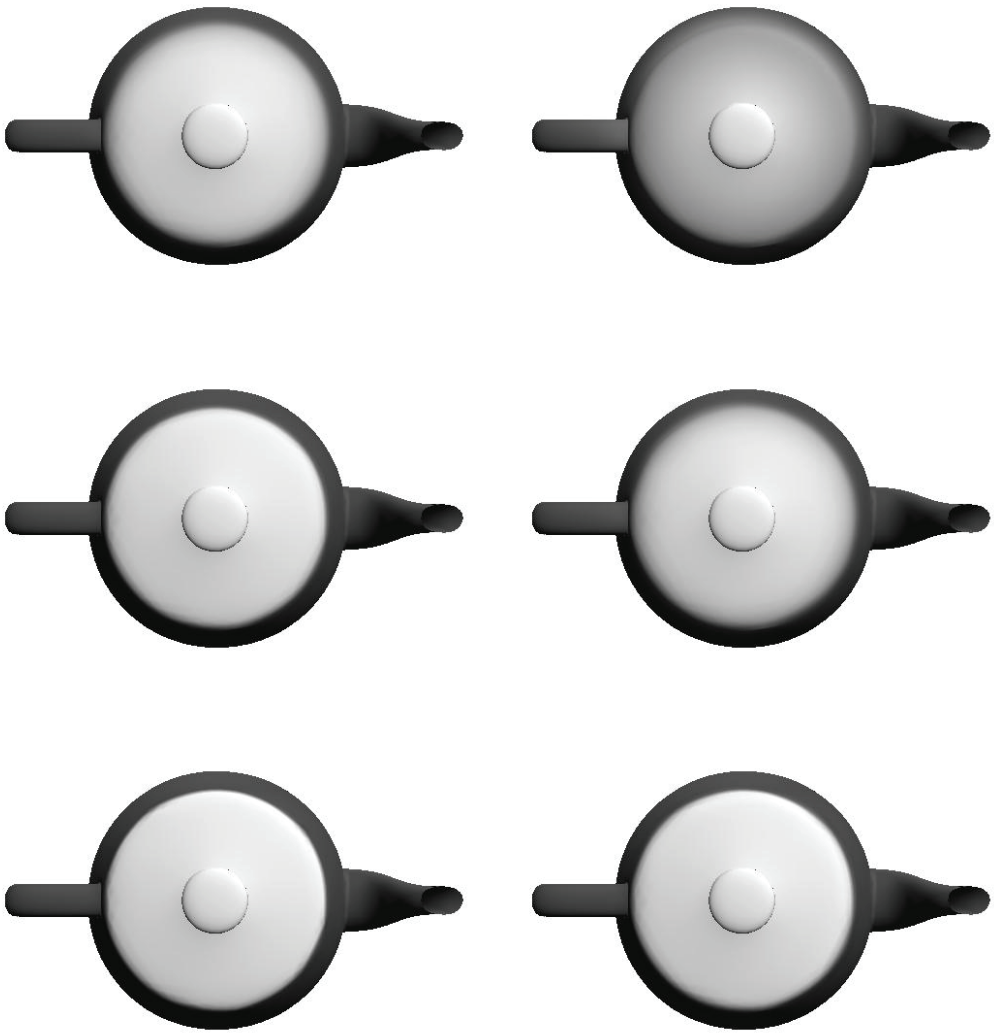

**Figure 14.** *Discrete anisotropic scale-spaces of an image on the Utah teapot model. Here* $e_1$ *is chosen to be the top-bottom direction on the tangent space of the teapot surface.* $e_2$ *is orthogonal to* $e_1$*. First row:* $g_1 = g_2 = 1$*. Second row:* $g_1 = 0.1$*,* $g_2 = 1$*. Third row:* $g_1 = 0$*,* $g_2 = 1$*. Left to right: with scales* 9*,* 100*, respectively.*

discrete filtering procedures of vector-valued data in order to construct and understand multiresolution representations of coupled multichannel information. Also, similar analysis can be applied to filtering of the mesh point coordinates of triangulated surfaces, that is, various mesh motions such as mean curvature flow and anisotropic geometric diffusion of mesh surfaces used in many discrete geometry processing and modelling applications. Another future work is the construction of discrete filtering and its analysis for images over other types of mesh surfaces although the nonsimplicial structure will bring some difficulties. In addition, the

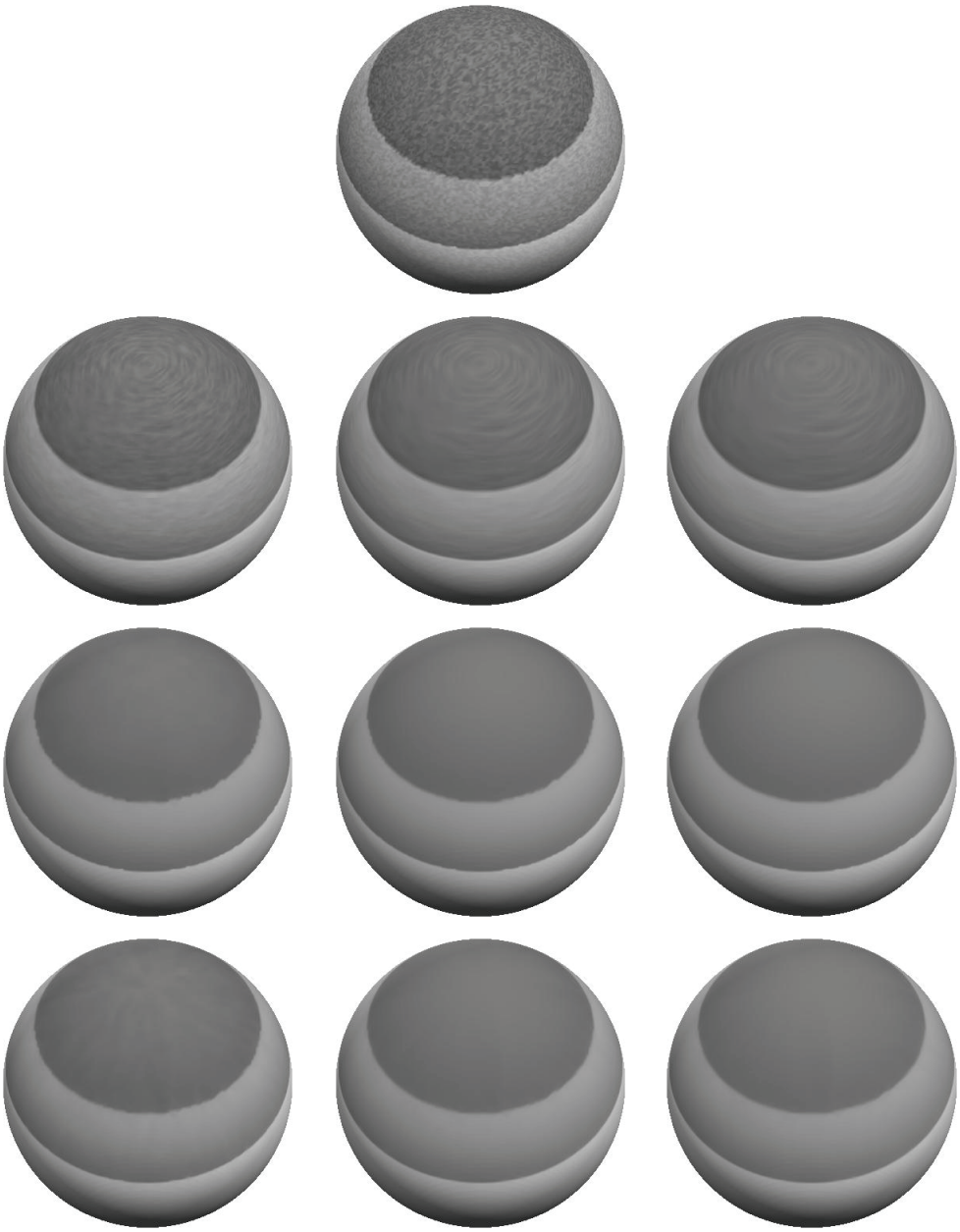

**Figure 15.** *Discrete anisotropic scale-spaces for anti-aliasing and denoising. The first row is the initial image containing noise and zigzag aliasing, while the other three rows are three anisotropic scale-spaces.* $e_1$*: the longitude.* $e_2$*: the latitude. Second row:* $g_1(s) = 0$, $g_2(s) = 0.1$. *Third row:* $g_1(s) = g_2(s) = \frac{1}{\sqrt{s^2+\beta}}$, $\beta = 10^{-10}$. *Fourth row:* $g_1(s) = \frac{1}{\sqrt{s^2+\beta}}$, $g_2(s) = 0.1$, $\beta = 10^{-10}$. *From left to right: with scales* 2, 5, 7, *respectively.*

examples of the anisotropic filtering exhibit an anti-aliasing effect which is very useful in 3D painting applications. We also call for new discrete filtering operators satisfying the maximum-minimum principle for any triangulated surfaces.

## REFERENCES


[1] O. K. C. Au, C. L. Tai, L. G. Liu, and H. B. Fu, *Dual Laplacian editing for meshes*, IEEE Trans. Vis. Comput. Graph., 12 (2006), pp. 386–395.

[2] G. Aubert and P. Kornprobst, *Mathematical Problems in Image Processing: Partial Differential Equations and the Calculus of Variations*, 2nd ed., Appl. Math. Sci. 147, Springer-Verlag, New York, 2006.

[3] J. Babaud, A. Witkin, M. Baudin, and R. Duda, *Uniqueness of the Gaussian kernel for scale-space filtering*, IEEE Trans. Pattern Anal. Mach. Intell., 8 (1986), pp. 26–33.

[4] C. L. Bajaj and G. Xu, *Anisotropic diffusion of surfaces and functions on surfaces*, ACM Trans. Graph., 22 (2003), pp. 4–32.

[5] M. Bertalmio, L. T. Cheng, S. Osher, and G. Sapiro, *Variational problems and partial differential equations on implicit surfaces*, J. Comput. Phys., 174 (2001), pp. 759–780.

[6] E. Catmull and J. Clark, *Recursively generated B-spline surfaces on arbitrary topological meshes*, Comput. Aided Des., 10 (1978), pp. 350–355.

[7] F. Catté, P.-L. Lions, J.-M. Morel, and T. Coll, *Image selective smoothing and edge detection by nonlinear diffusion*, SIAM J. Numer. Anal., 29 (1992), pp. 182–193.

[8] T. F. Chan, S. Osher, and J. Shen, *The digital TV filter and nonlinear denoising*, IEEE Trans. Image Process., 10 (2001), pp. 231–241.

[9] T. Chan, S. Esedoglu, F. Park, and A. Yip, *Recent Developments in Total Variation Image Restoration*, CAM report 05-01, UCLA, Los Angeles, 2005; available online at ftp://ftp.math.ucla.edu/pub/camreport/cam05-01.pdf.

[10] U. Clarenz, U. Diewald, and M. Rumpf, *Anisotropic geometric diffusion in surface processing*, VIS '00: Proceedings of the Conference on Visualization, Salt Lake City, UT, IEEE Computer Society Press, Los Alamitos, CA, 2000, pp. 397–405.

[11] A. Cunha, R. Teixeira, and L. Velho, *Discrete scale spaces via heat equation*, in SIBGRAPI '01: Proceedings of the XIV Brazilian Symposium on Computer Graphics and Image Processing, IEEE Computer Society, Washington, DC, 2001, pp. 68–75.

[12] M. Desbrun, M. Meyer, P. Schröder, and A. H. Barr, *Implicit fairing of irregular meshes using diffusion and curvature flow*, in SIGGRAPH99: Proceedings of the 26th Annual Conference on Computer Graphics and Interactive Techniques, ACM Press, Addison–Wesley, New York, 1999, pp. 317–324.

[13] L. M. J. Florack, *Image Structure*, Kluwer Academic Publishers, Springer-Verlag, Dordrecht, The Netherlands, 1997.

[14] L. Florack and A. Kuijper, *The topological structure of scale-space images*, J. Math. Imaging Vision, 12 (2000), pp. 65–80.

[15] P. M. Gandoin and O. Devillers, *Progressive lossless compression of arbitrary simplicial complexes*, ACM Trans. Graph., 21 (2002), pp. 372–379.

[16] A. N. Hirani, *Discrete Exterior Calculus*, Ph.D. thesis, California Institute of Technology, Pasadena, CA, 2003.

[17] R. A. Horn and C. R. Johnson, *Matrix Analysis*, Cambridge University Press, Cambridge, UK, 1985.

[18] A. Hummel, *Representations based on zero-crossings in scale-space*, in Readings in Computer Vision: Issues, Problems, Principles, and Paradigms, M. Fischler and O. Firschein, eds., Morgan Kaufmann, Los Altos, CA, 1987, pp. 753–758.

[19] S. L. Keeling and R. Stollberger, *Nonlinear anisotropic diffusion filtering for multiscale edge enhancement*, Inverse Problems, 18 (2002), pp. 175–190.

[20] S. Kichenassamy, *The Perona–Malik paradox*, SIAM J. Appl. Math., 57 (1997), pp. 1328–1342.

[21] B. B. Kimia and K. Siddiqi, *Geometric heat equation and nonlinear diffusion of shapes and images*, Comput. Vis. Image Underst., 64 (1996), pp. 305–322.

[22] R. Kimmel, *Intrinsic scale space for images on surfaces: The geodesic curvature flow*, Graph. Models Image Process., 59 (1997), pp. 365–372.

[23] J. Koenderink, *The structure of images*, Biol. Cybern., 50 (1984), pp. 363–370.

[24] J. J. Koenderink and A. J. van Doorn, *Generic neighborhood operators*, IEEE Trans. Pattern Anal. Mach. Intell., 14 (1992), pp. 597–605.

[25] G. Kühne, J. Weickert, M. Beier, and W. Effelsberg, *Fast implicit active contour models*, in Proceedings of the 24th DAGM Symposium on Pattern Recognition, Lecture Notes in Comput. Sci. 2449, Springer-Verlag, London, 2002, pp. 133–140.
[26] A. Kuijper and L. M. J. Florack, *The relevance of non-generic events in scale space models*, Int. J. Comput. Vision, 57 (2004), pp. 67–84.
[27] A. Kuijper and L. M. J. Florack, *Understanding and modeling the evolution of critical points under Gaussian blurring*, in Proceedings of the 7th European Conference on Computer Vision 2002, Part I, Copenhagen, Denmark, Springer-Verlag, Berlin, 2002, pp. 143–157.
[28] A. Kuijper, L. M. J. Florack, and M. A. Viergever, *Scale space hierarchy*, J. Math. Imaging Vision, 18 (2003), pp. 169–189.
[29] T. Leung and J. Malik, *Representing and recognizing the visual appearance of materials using three-dimensional textons*, Int. J. Comput. Vision, 43 (2001), pp. 29–44.
[30] G. Lin and P. Y. Yu, *An improved vertex caching scheme for 3D mesh rendering*, IEEE Trans. Vis. Comput. Graph., 12 (2006), pp. 640–648.
[31] T. Lindeberg, *Scale-space for discrete signals*, IEEE Trans. Pattern Anal. Mach. Intell., 12 (1990), pp. 234–254.
[32] T. Lindeberg, *Scale-space behaviour of local extrema and blobs*, J. Math. Imaging Vision, 1 (1992), pp. 65–99.
[33] T. Lindeberg, *Scale-Space Theory in Computer Vision*, Kluwer Academic Publishers, Dordrecht, The Netherlands, 1994.
[34] T. Lindeberg, *On the axiomatic foundations of linear scale-space*, in Gaussian Scale Space Theory, J. Sporring et al., eds., Kluwer Academic Publishers, Dordrecht, The Netherlands, 1996, pp. 75–98.
[35] T. Lindeberg, *Scale-space: A framework for handling image structures at multiple scales*, in Proceedings of CERN School of Computing, Egmond aan Zee, The Netherlands, 1996, pp. 1–12; available online at http://www.nada.kth.se/cvap/abstracts/lin96-csc.html.
[36] T. Lindeberg, *Feature detection with automatic scale selection*, Int. J. Comput. Vision, 30 (1998), pp. 77–116.
[37] T. Lindeberg, *Scale-space*, in Encyclopedia of Computer Science and Engineering, IV, B. Wah, ed., John Wiley and Sons, Hoboken, NJ, 2009, pp. 2495–2504; available online at http://www.nada.kth.se/~tony/abstracts/Lin08-EncCompSci.html.
[38] D. G. Lowe, *Distinctive image features from scale-invariant keypoints*, Int. J. Comput. Vision, 60 (2004), pp. 91–110.
[39] T. Lu, P. Neittaanmäki, and X.-C. Tai, *A parallel splitting up method and its application to Navier-Stokes equations*, Appl. Math. Lett., 4 (1991), pp. 25–29.
[40] J. E. Marsden, T. Ratiu, and R. Abraham, *Manifolds, Tensor Analysis, and Applications*, 3rd ed., Springer-Verlag, New York, 2002.
[41] M. Meyer, M. Desbrun, P. Schröder, and A. Barr, *Discrete differential-geometry operator for triangulated 2-manifolds*, in Visualization and Mathematics III, Math. Vis., Springer-Verlag, Berlin, 2003, pp. 35–57.
[42] K. Mikolajczyk and C. Schmid, *Scale and affine invariant interest point detectors*, Int. J. Comput. Vision, 60 (2004), pp. 63–86.
[43] N. Paragios, Y. Chen, and O. Faugeras, *Handbook of Mathematical Models in Computer Vision*, Springer-Verlag, New York, 2005.
[44] P. Perona and J. Malik, *Scale-space and edge detection using anisotropic diffusion*, IEEE Trans. Pattern Anal. Mach. Intell., 12 (1990), pp. 629–639.
[45] A. Petrovic, O. D. Escoda, and P. Vandergheynst, *Multiresolution segmentation of natural images: From linear to non-linear scale-space representations*, IEEE Trans. Image Process., 13 (2004), pp. 1104–1114.
[46] G. Poole and T. Boullion, *A survey on M-matrices*, SIAM Rev., 16 (1974), pp. 419–427.
[47] L. Rudin, S. Osher, and E. Fatemi, *Nonlinear total variation based noise removal algorithms*, Phys. D, 60 (1992), pp. 259–268.
[48] T. Sakai and A. Imiya, *Gradient structure of image in scale space*, J. Math. Imaging Vision, 28 (2007), pp. 243–257.
[49] L. Shi and Y. Yu, *Inviscid and incompressible fluid simulation on triangle meshes*, Comput. Animat. Virtual Worlds, 15 (2004), pp. 173–181.

[50] O. Sorkine, D. Cohen-Or, R. Goldenthal, and D. Lischinski, *Bounded-distortion piecewise mesh parameterization*, in VIS '02: Proceedings of the Conference on Visualization '02, IEEE Computer Society, Washington, DC, 2002, pp. 355–362.

[51] J. Sporring, *The entropy of scale-space*, in Proceedings of the 1996 International Conference on Pattern Recognition (ICPR), IEEE Computer Society, Washington, DC, 1996, pp. 900–904.

[52] J. Sporring and O. F. Olsen, *Segmenting by compression using linear scale-space and watersheds*, in Scale-Space Theories in Computer Vision, Lecture Notes in Comput. Sci. 1682, Springer-Verlag, Berlin, 1999, pp. 513–518.

[53] J. Stam, *Flows on surfaces of arbitrary topology*, ACM Trans. Graph., 22 (2003), pp. 724–731.

[54] G. Taubin and J. Rossignac, *Geometric compression through topological surgery*, ACM Trans. Graph., 17 (1998), pp. 84–115.

[55] J. Weickert, *Scale-Space Properties of Nonlinear Diffusion Filtering with a Diffusion Tensor*, Technical report 110, Laboratory of Technomathematics, University of Kaiserslautern, Kaiserslautern, Germany, 1994.

[56] J. Weickert, *Nonlinear diffusion scale-spaces: From the continuous to the discrete setting*, in ICAOS: Images, Wavelets, and PDEs, Paris, 1996, Springer-Verlag, London, 1996, pp. 111–118.

[57] J. Weickert and B. Benhamouda, *A semidiscrete nonlinear scale-space theory and its relation to the Perona-Malik paradox*, in Advances in Computer Vision, Springer-Verlag, Wien, 1997, pp. 1–10.

[58] J. Weickert, *Anisotropic Diffusion in Image Processing*, Teubner, Stuttgart, Germany, 1998.

[59] T. J. Willmore, *Riemannian Geometry*, Oxford Science Publications, The Clarendon Press, Oxford University Press, New York, 1993.

[60] A. P. Witkin, *Scale-space filtering*, in Proceedings of the 8th International Joint Conference on Artificial Intelligence, Karlsruhe, Germany, 1983, pp. 1019–1022; available online at http://dli.iiit.ac.in/ijcai/IJCAI-83-VOL-2/PDF/091.pdf.

[61] C. Wu, J. Deng, and F. Chen, *Diffusion equations over arbitrary triangulated surfaces for filtering and texture applications*, IEEE Trans. Vis. Comput. Graph., 14 (2008), pp. 666–679.

[62] Y. L. You, W. Y. Xu, A. Tannenbaum, and M. Kaveh, *Behavioral analysis of anisotropic diffusion in image processing*, IEEE Trans. Image Process., 5 (1996), pp. 1539–1553.

[63] Y. Z. Yu, K. Zhou, D. Xu, X. H. Shi, H. J. Bao, B. N. Guo, and H. Y. Shum, *Mesh editing with Poisson-based gradient field manipulation*, ACM Trans. Graph., 23 (2004), pp. 644–651.

[64] A. Yuille and T. Poggio, *Scaling theorems for zero crossings*, IEEE Trans. Pattern Anal. Mach. Intell., 8 (1986), pp. 15–25.

[65] E. Zhang, K. Mischaikow, and G. Turk, *Feature-based surface parameterization and texture mapping*, ACM Trans. Graph., 24 (2005), pp. 1–27.

[66] D. Zorin and P. Schroder, *Subdivision for Modeling and Animation*, SIGGRAPH 2000 Course Notes, ACM Press, New York, 2000.